Zoologischer Anzeiger
November 2022, Volume 301, Pages 23-41
https://doi.org/10.1016/j.jcz.2022.09.001
https://archimer.ifremer.fr/doc/00793/90500/

Two new species of mud dragons (Scalidophora: Kinorhyncha) inhabiting a human-impacted mangrove from Mayotte (Southwestern Indian Ocean)

Cepeda Gomez Diego [1, *], González-Casarrubios Alberto [2], Sánchez Nuria [2], Spedicato Adriana [3], Michaud Emma [3], Zeppilli Daniela [1]

[1] Deep-Sea Laboratory (LEP), French Institute for Ocean Science (IFREMER), ZI de La Pointe du Diable, CS 10070, 29280, Plouzané, France
[2] Complutense University of Madrid (UCM), Faculty of Biology, Department of Biodiversity, Ecology and Evolution (BEE), C/ José Antonio Novais 12, 28040, Madrid, Spain
[3] University of Western Brittany (UBO), French National Centre for Scientific Research (CNRS), Research Institute for Development (IRD), IFREMER, Laboratory of Sciences of Marine Environment (LEMAR), F-29280, Plouzané, France

* Corresponding author : Diego Cepeda Gomez, email address : dcepedag@ifremer.fr

Abstract :

The Kinorhyncha community inhabiting a mangrove forest impacted by domestic sewage discharges in the past has been explored in Mayotte Archipelago (southwestern Indian Ocean). Two new species of Echinoderes, which putatively belong to the Echinoderes coulli-group, are described: E. cyaneafictus sp. nov. And E. parthenope sp. nov. Echinoderes cyaneafictus sp. nov. has short, poorly sclerotized, weakly articulated spines in middorsal position on segment 4 and sublateral position on segments 6–7, plus tubes in lateroventral position on segment 5, lateral accessory position on segment 8 and laterodorsal position on segment 10. Echinoderes parthenope sp. nov. has the same kind of spines in middorsal position on segment 4, lateroventral position on segment 6, sublateral position on segment 7 and lateral accessory position on segment 8, plus tubes in lateroventral position on segments 5 and 8 and laterodorsal position on segment 10 (only males). Both species are characterized by having an enlarged sieve plate (nephridiopore) consisting of an anterior, convex area with numerous pores and a posterior, concave region with a single pore, which characterizes the species group. This combination of characters, together with their intertidal environment affected by strong salinity fluctuations, led us to assign both species to the E. coulli-group tentatively. Apart from these characters, the new species possess a unique combination of morphological features that unambiguously differentiates them from their congeners. The studied kinorhynch community seems not to be negatively affected by the domestic sewage emissions from the nearby town Malamani. We did not find evidence for significant differences in density or richness between the area more impacted by this pollution and the pristine area.

Keywords : Kinorhynchs, Anthropic influence, Echinoderes, Mangrove forests, Taxonomy, Pollution.

1. Introduction

Mangroves are extreme habitats with great variations in water level, salinity, temperature, pH and available oxygen at both spatial and temporal scales (Hogarth 1999; Kathiresan & Bingham 2001). These forests offer a wide range of environmental services and have a high economic and ecological importance (Saenger 2002).

On the biological side, vegetation composition of mangroves varies from one place to another around the world, and recent studies demonstrated the hosted communities of associated organisms are relatively poor in diversity compared to other coastal ecosystems (Alongi 2002; Gilman et al. 2008; Xie et al. 2020). Sediment supporting mangroves usually shelters different meiofaunal organisms (Edgar 1990; Sasekumar & Chong 1998; Kathiresan & Bingham 2001). This sediment is frequently compacted, with high content of litter, easily becoming acidic and anaerobic, which makes it a challenging environment to live in (Sukardjo 1994). In addition to these natural conditions, mangroves are also defiant in the sense of being recurrently affected by human activities because of their vicinity with towns, industries, aquatic farms and harbours. Meiofauna, as a component of marine benthos, is affected by direct contact with potential pollutants that may accumulate in mangrove sediments, including heavy metals, oil spills, organic compounds or sewage (Bartolini et al. 2011; Lewis et al. 2011; Molnar et al. 2013; Zhang et al. 2014; Della Patrona et al. 2016; Duke 2016; Michelet et al. 2021).

Meiofaunal communities of mangroves are mainly dominated by nematodes, harpacticoid copepods, annelids (especially oligochaetes) and, according to studies based on eDNA analyses, flatworms (Alongi 1987, 1990; Somerfield et al. 1998; Kathiresan & Bingham 2001; Nagelkerken et al. 2008; Fonseca et al. 2010). However, other less common meiofauna may also be found at this particular environment at abundances of typically <5%, including Kinorhyncha (Hodda & Nicholas 1986; Schrijvers et al. 1997; Mokievsky et al. 2011; Della Patrona et al. 2016; Khalil 2019; Michelet et al. 2021). Exceptionally, kinorhynchs may reach higher levels of density in mangroves, being within the top three dominant groups, with values of 39–117 ind/10cm^2 (Gomes et al. 2002; Santos et al. 2009; Ostmann et al. 2012; Annapurna et al. 2015).

Mangrove sediments are not among the most colonized environments by kinorhynchs, but certain species are able to benefit from their conditions. Some of the main environmental factors that seem to configure kinorhynch communities in mangroves

are prokaryotic community composition, percentages of silt and clay, solar radiation, pigments and pollutants (Gomes et al. 2002; Santos et al. 2009; Ostmann et al. 2012; Annapurna et al. 2015; Della Patrona et al. 2016; Michelet et al. 2021). Currently, 39 out of the 313 recognized kinorhynch species have been found living in mangrove sediments (Table 1). Although some of these have only been found in mangrove areas (*e.g. E. applicitus* Ostmann et al., 2012; *E. komatsui* Yamasaki & Fujimoto, 2014), most of them may be found (even at higher densities) in other kinds of habitats.

On the other hand, some species seem to share morphological specializations presumably adapted to cope with the particular environmental conditions of the mangroves, i.e., *Echinoderes bengalensis* (Timm, 1958), *E. caribiensis* Kirsteuer, 1964, *E. komatsui*, *E. strii* Pardos et al., 2016 (in Pardos et al. 2016a) and *E. teretis* Brown 1999 in Adrianov & Malakhov, 1999. These species belong to the *E. coulli*-group, and are characterized by having an enlarged nephridiopore that forms a sieve plate with numerous pores. These sieve plates have been interpreted as an adaptation to life at the low salinity levels mangroves may reach, by increasing the osmoregulation efficiency (Ostmann et al. 2012; Zeppilli et al. 2016; Randsø et al. 2019). Although this kind of nephridiopore also appears in other congeners that do not live in mangrove areas, it could still be an advantage for the species living in intertidal, highly fluctuating salinity waters (Lundbye et al. 2011; Yamasaki 2016).

A new meiofauna survey done at Mayotte, Indian Ocean, has revealed two new species of *Echinoderes* Claparède, 1863 inhabiting muddy sediments in a mangrove area. The aim of the present paper is to formally describe the two species and discuss relevant systematic and ecological remarks of the new species and their environment.

2. Material and methods

2.1 Study site and sampling.

Samples of the present study, consisting of black organic mud, were obtained on October 6th, 2018, at 9h15–15h30 in a large mangrove swamp (ca. 650ha) during the dry season and low tide at Chirongui Bay, Grande-Terre Island, Mayotte Archipelago (Mozambique Channel, SW Indian Ocean) (Fig. 1A-C). The forest was structured in four distinct areas, each one dominated by a different mangrove tree arranged in approximately parallel

bands to the sea, from the farthest to the closest zone to the shore in the following way: the *Avicennia marina* (Forssk.) Vierh. area, the *Ceriops tagal* (Perr.) C.B. Robinson area, the *Rhizophora mucronata* Lam. area, and the *Sonneratia alba* area Sm. (Fig. 1D-E) (see Herteman et al. 2011 for more detailed information on the forest structure and composition).

The mangrove swamp was affected by domestic sewage discharge from the nearby village Malamani (ca. 800 inhabitants) (Fig. 1D-E) during 10 years (2008–2018). Sewage inputs were characterized by high levels of organic matter, nitrogen (mainly ammonium) and phosphorus compounds (see Capdeville et al. 2018, 2019 for more detailed information on the physicochemical parameters in water and sediment). It must be noticed that the sewage discharges in the mangrove only occurred right before the present experiment, and they were rather occasional during the sampling.

The present study was conducted in the *Rhizophora mucronata* area, where two sites were selected for sediment sampling: the "control" site, further apart from the wastewater pipe and presumably less polluted (12°55'22.8"S, 45°09'09.1"E), and the "impacted" site, directly in the zone affected by the sewage discharge (12°55'17.5"S, 45°09'10.4"E) (Fig. 1D). Previous studies determined significant differences for nitrogen (NO_3^-, NO_2^- and NH_4^+) and phosphorus (PO_4^{3-}) compounds between the two kinds of sites, concluding that the "impacted" plot was affected by higher concentrations of organic matter derived from sewage discharge (Capdeville et al. 2018, 2019). On each site, three sediment cores (10cm diameter, 18cm height) were randomly selected, and subsamples of sediment (1.76cm^2) were taken at different layers for each core: the surface layer (0–2cm, volume of subsample 3.5cm^3) and the deep layer (2–10cm, volume of subsample 14cm^3), as meiofauna is more abundant in the upper, well-oxygenized sediment layers (Coull 1988).

2.2 Extraction and preparation of meiofaunal organisms.

Each subsample was fixed in 4% buffered formalin (mineral water, NaCl 33g·L^{-1}). Once at the laboratory, each subsample was passed through a 1000µm sieve (for macrofauna extraction), then through a 30µm sieve, and rinsed to remove formaldehyde leftovers. Meiofauna from the subsamples was finally extracted by LUDOX® colloidal silica

153 centrifugation following the procedures of Heip et al. (1985), and meiofaunal organisms
154 were preserved in 4% formalin.

155 To identify meiofaunal organisms, erythrosine ($8g \cdot L^{-1}$) was used to stain the
156 individuals for 24h. Organisms were separated by phylum and kinorhynchs were prepared
157 for microscopy study. For light microscopy (LM), kinorhynchs were rinsed with distilled
158 water to remove formaldehyde remnants, passed through a graded series of glycerine,
159 kept in a solution of 100% glycerine for at least 24h and mounted on glass slides using
160 Fluoromount G®. Mounted, adult specimens were identified to the genus level using an
161 Olympus© BX51-P differential interference contrast microscopy with the dichotomous
162 key provided by Sørensen & Pardos (2020). An Olympus© DP-70 camera was used to
163 photograph the specimens. For scanning electron microscopy (SEM), kinorhynchs were
164 rinsed with distilled water to remove formalin remnants and passed through a graded
165 series of ethanol, then through a graded series of acetone. Finally, specimens were
166 critical-point dried, mounted on aluminum stubs and sputter-coated with gold-palladium
167 for 90s for examination with a JEOL© JSM-6335F field emission scanning electron
168 microscope at the Spanish National Centre for Electron Microscopy (ICTS, Complutense
169 University of Madrid, Spain).

170 Line art drawings of the new species and micrographs were prepared and
171 composed using Adobe® Photoshop and Illustrator CS6 software. Type and additional
172 material for LM was deposited at the Muséum National d'Histoire Naturelle (MNHN),
173 France.

174

175 *2.3 Statistical analyses.*

176 Kruskal-Wallis analyses were used to assess differences in kinorhynch richness and
177 density between the two kinds of environments ("control" vs. "impacted") in R v.6.3.1
178 software (R Core Team 2021). This non-parametric analysis is intuitively similar to an
179 ANOVA with the data replaced by categories and without assuming a normal distribution
180 of the data and homogeneous variances.

181 Changes through the vertical profile (i.e. between the upper and the lower layers
182 of the cores) could not be assessed, as kinorhynchs were only recovered at the upper,
183 more-oxygenated layer.

3. Results

Taxonomic account

Class **Cyclorhagida** (Zelinka, 1896) Herranz et al., 2022

Family **Echinoderidae** Carus, 1885

Genus ***Echinoderes*** Claparède, 1863

3.1 *Echinoderes cyaneafictus* sp. nov.

Zoobank code: urn:lsid:zoobank.org:act:AD7E82A4-F389-485E-8B7B-2E53437B09C1

(Figs. 2–4, Tables 2–3)

3.1.1 Material examined

Holotype, adult male, collected in October 6th, 2018, at Chirongui Bay, Grande-Terre Island, Mayotte Archipelago, SW Indian Ocean: 12°55'17.5"S, 45°09'10.4"E–12°55'22.8"S, 45°09'09.1"E in black organic mud at the intertidal zone; mounted in Fluoromount G®, deposited at MNHN under catalogue number: 623Ma. Paratypes, 23 adult males and 14 adult females, same collecting data as holotype; mounted in Fluoromount G®, deposited at MNHN under catalogue numbers: 587Ma-589Ma, 594Ma-595Ma, 597Ma-599Ma, 601Ma-606Ma, 608Ma-612Ma, 614Ma, 616Ma, 618Ma-620Ma, 622Ma, 626Ma-628Ma and 630Ma-636Ma. Additional, non-type material: 12 juveniles, same collecting data as holotype and paratypes; mounted in Fluoromount G®, deposited at MNHN under catalogue numbers: 590Ma-593Ma, 596Ma, 600Ma, 607Ma, 615Ma, 617Ma, 621Ma and 624Ma-625Ma.

3.1.2 Diagnosis

Echinoderes with spines that are short, poorly sclerotized and weakly articulated in middorsal position on segment 4 and sublateral position on segments 6–7, plus large tubes in lateroventral position on segment 5, lateral accessory position on segment 8 and laterodorsal position on segment 10. Enlarged, oval sieve plate openings in sublateral position on segment 9, consisting of an anterior, slightly convex region bearing numerous pores, and a posterior, slightly concave area bearing a single pore.

3.1.3 Etymology

The species name derives from *Cyanea* Péron & Lesueur, 1810, which is a genus of scyphozoan cnidarians characterized by having multiple, elongated tentacles (resembling the elongated hairs of the segment 1 sensory spots of the species) and the Latin *fictus* (meaning feigned, false, counterfeit).

3.1.4 Description

See Table 2 for measurements of selected morphological traits and dimensions, and Table 3 for summary of acicular spine, tube, nephridiopore, glandular cell outlet and sensory spot locations.

Head: only a few specimens were found with a completely everted head, hence only a few details in some structures can be provided. Ring 00 of mouth cone with nine outer oral styles alternating in size between slightly larger and smaller ones. Outer oral styles composed of two jointed subunits: a rectangular, basal piece with proximal fringed sheath bearing a tuft of 5–7 spinous processes; and a triangular, hooked, distally pointed and curved end-piece (Fig. 3F). Triangular, strongly sclerotized, basally fringed cuticular thickenings flanking the outer oral styles. Outer oral styles located anterior to each introvert sector, except in the middorsal sector 6.

Introvert with six rings of scalids (one ring of primary spinoscalids and five rings of regular-sized scalids) and 10 longitudinal sectors delimited by the arrangement of the primary spinoscalids. Ring 01 of introvert with 10 primary spinoscalids, larger than remaining ones, laterally compressed, composed of a medially fringed basal sheath and a distal, elongated, flexible, distally blunt end-piece (Fig. 3F). Remaining rings of introvert with regular-sized scalids, composed of a rectangular basal sheath and a distal, elongated, acicular, distally pointed end-piece (Fig. 3F). Scalids tend to collapse when mounted for LM (Fig. 3F), and specimens for SEM were not available, so details on the scalid arrangement are not provided.

Neck: 16 trapezoidal placids, wider at base, closely adjacent, with distinct joint between the neck and first trunk segment. Midventral placid widest (ca. 9–10 μm wide at base), remaining ones slightly narrower (ca. 6–8 μm wide at base). A ring of six long, superficially haired trichoscalids associated with the placids, attached to large, bottle-shaped trichoscalid plates (Figs. 2A-B, D-E; 3B, D, F).

Trunk: fusiform, composed of 11 segments, heart-shaped in cross-section. Segments 1–2 closed, ring-like cuticular plates, remaining ones with one tergal and two sternal cuticular plates (Figs. 2A-B, D-E; 3A; 4A). Maximum sternal width at segment 7, trunk progressively tapering toward anterior and posterior ends. Cuticular hairs throughout segments 2–10, emerging from rounded to slightly oval perforation sites. Cuticular hairs arranged as 6–8 approximately straight transversal rows densely covering the cuticular surface of segment 2; as 5–7 transversal, uninterrupted rows that become wavy at laterodorsal, sublateral and ventrolateral to ventromedial regions on segment 3; as 7–12 transversal rows interrupted at the laterodorsal region that become wavy at sublateral and ventrolateral to ventromedial regions on segments 4–10; segments 1 and 11 without hairs (Figs. 2A-E; 3B-D; 4B-F). Posterior segment margins straight, with a long, conspicuous, strongly serrated primary pectinate fringe (Figs. 2A-E; 3B-C; 4B-F). Secondary pectinate fringes not detected.

Segment 1: type 1 glandular cell outlets in middorsal and lateroventral positions, the former near the anterior segment margin, the latter located at the anterior half of the segment (Figs. 2A-E; 3B). Rounded sensory spots (sensu Lundbye et al. 2011) in subdorsal, laterodorsal and ventrolateral positions, the former two located near the anterior segment margin, the latter located near the posterior segment end; these sensory spots are characterized by having the posterior part of the papillae area with a transversal row of conspicuously elongated hairs (Figs. 2A-B, D-E; 3B, D, E).

Segment 2: type 1 glandular cell outlets in middorsal and ventromedial positions (Fig. 2A-B, D-E; 3D). Droplet-shaped sensory spots (*sensu* Lundbye et al. 2011) in middorsal position only in males, in paradorsal and midlateral positions only in females, and also in subdorsal and laterodorsal positions in both sexes (Figs. 2A-B, D-E; 3B).

Segment 3: type 1 glandular cell outlets in middorsal and ventromedial positions (Fig. 2A-B, D-E; 3D). Droplet-shaped sensory spots in middorsal and subdorsal positions, and also in midlateral position only in females (Figs. 2B, D-E).

Segment 4: short (ca. 4–10 μm long), poorly sclerotized, weakly articulated, acicular spine in middorsal position (Figs. 2B; 3B). Type 1 glandular cell outlets in paradorsal and ventromedial positions (Fig. 2A-B).

Segment 5: tubes in lateroventral position (Figs. 2A; 3C). Type 1 glandular cell outlets in paradorsal and ventromedial positions (Figs. 2A-B; 4B). Droplet-shaped sensory spots in subdorsal, midlateral and ventromedial positions (Figs. 2A-B; 3C; 4B).

Segment 6: short (ca. 4–7 μm long), poorly sclerotized, weakly articulated, acicular spines in sublateral position (Figs. 2A; 3C). Type 1 glandular cell outlets in paradorsal and ventromedial positions (Figs. 2A-B; 4B). Droplet-shaped sensory spots in subdorsal, midlateral and ventromedial positions, the former slightly more mesial than those of the precedent segment but still in subdorsal position (Figs. 2A-B; 3C; 4B).

Segment 7: similar to segment 6 in the arrangement of spines, glandular cell outlets and sensory spots (Figs. 2A-B; 3C; 4B).

Segment 8: tubes in lateral accessory position (Figs. 2A; 3C). Type 1 glandular cell outlets in paradorsal and ventromedial positions (Figs. 2A-B; 4B-C). Droplet-shaped sensory spots in paradorsal and ventrolateral positions (Figs. 2A-B; 4B-C).

Segment 9: type 1 glandular cell outlets in paradorsal and ventromedial positions (Figs. 2A-B; 4C). Droplet-shaped sensory spots in paradorsal, subdorsal and ventrolateral positions (Figs. 2A-B; 4C). Nephridiopores in sublateral position as oval, enlarged sieve plate openings consisting of an anterior, elongated, slightly convex area with numerous pores, and a posterior, slightly concave region with a single pore (*sensu* Lundbye et al. 2011) (Figs. 2A; 4F).

Segment 10: tubes in laterodorsal position (Fig. 2B). Two longitudinally aligned type 1 glandular cell outlets in middorsal position; type 1 glandular cell outlets also in ventromedial position (Figs. 2A-C; 4C, E). Droplet-shaped sensory spots in subdorsal and ventrolateral positions (Figs. 2A-C; 4C, E). Posterior margins of sternal plates midventrally extended, forming an elongated, V-shaped extension over the following segment (Figs. 2A; 4D-E).

Segment 11: relatively short lateral terminal spines (LTS:TL average ratio = 23.8%), apparently well sclerotized but still quite flexible, distally pointed, with a hollow central cavity (Figs. 2A-C; 3A; 4A, D-E). Males with three pairs of penile spines, dorsal and ventral pairs longer and slender, smooth and distally rounded, medial pair shorter and stouter, hairy with a distal tuft of hairs (Figs. 2A-B; 4E); females with short (LTAS:LTS average ratio = 5.0%), slender, occasionally distally frayed, lateral terminal accessory

spines (Figs. 2C; 4D). Type 1 glandular cell outlet in middorsal position (Fig. 2B-C). Rounded sensory spots in subdorsal and ventromedial positions, the latter near the basal insertion of the lateral terminal spines (Figs. 2A-C; 4E). Tergal extensions forming projections laterally, with blunt tips in males and pointed tips in females; posterior margin between the tergal extensions densely fringed (Figs. 2A-C; 4D-E). Sternal extensions short, distally rounded (Figs. 2A; 4E).

3.1.5 Remarks

The holotype of the species (MNHN-623Ma) was found carrying epibiont, filamentous bacteria attached to the lateral margins of segment 11 tergal plate (Fig. 3A).

3.2 ***Echinoderes parthenope*** **sp. nov.**

Zoobank code: urn:lsid:zoobank.org:act:4E6BFE9E-D25F-4A91-99F0E5D47E37BA91

(Figs. 5–9, Tables 4–5)

3.2.1 Material examined

Holotype, adult male, collected in October 6th, 2018, at Chirongui Bay, Grande-Terre Island, Mayotte Archipelago, SW Indian Ocean: 12°55'17.5"S, 45°09'10.4"E–12°55'22.8"S, 45°09'09.1"E in black organic mud at the intertidal zone; mounted in Fluoromount G®, deposited at MNHN under catalogue number: 613Ma. Paratypes, five adult males and one adult female, same collecting data as holotype; mounted in Fluoromount G®, deposited at MNHN under catalogue numbers: 637Ma, 641Ma-643Ma, 649Ma and 651Ma. Additional material, one adult male, same collecting data as type material; mounted for SEM, stored at the Meiofauna collection of the UCM; 10 juveniles, same collecting data as type material, deposited at MNHN under catalogue numbers: 638Ma-640Ma, 644Ma-648Ma, 650Ma and 652Ma.

3.2.2 Diagnosis

Echinoderes with spines that are short, poorly sclerotized, weakly articulated in middorsal position on segment 4, lateroventral position on segment 6, sublateral position on segment 7 and lateral accessory position on segment 8, plus large tubes in lateroventral position on segment 5, sublateral position on segment 8 and laterodorsal position on segment 10 (only in males). Minute, rounded type 2 glandular cell outlets in subdorsal position on

segments 5–6, in laterodorsal position on segment 9, in midlateral position on segment 4, in sublateral position on segment 7, and in lateral accessory position on segment 6. Enlarged, triangular sieve plates in sublateral position on segment 9, consisting of a slightly convex region bearing numerous pores followed by a small, slightly concave area bearing a single, enlarged pore. Males with tergal plate of segment 10 forming a pair of cuticular, rectangular extensions in subdorsal position, with straight, abruptly tapering, slightly curved tips; females with tufts of hairs instead. Males with tergal plate of segment 11 forming a middorsal, triangular, bulged process that extends slightly beyond the tergal extensions.

3.2.3 Etymology

The species is dedicated to the Greek, mythological mermaid *Parthenope* (from the Ancient Greek *Παρθενόπη*). *Parthenope* gave name to the first Greek settlement now part of the Italian city of Naples. According to legend, *Parthenope* despaired after failing to lure Odysseus to her island, cast herself into the sea and drowned, her body washed ashore near Naples. The mermaid is usually represented in art with two tails, which resembles in shape the characteristic segment 11 tergal plate of the species.

3.2.4 Description

See Table 4 for measurements of selected morphological traits and dimensions, and Table 5 for summary of acicular spine, tube, nephridiopore, glandular cell outlet, sensory spot, hair tuft and cuticular extension locations.

Head: a single specimen for LM was found with a completely everted head, hence only a few details in some structures can be provided. Ring 00 of mouth cone with nine outer oral styles alternating in size between slightly larger and smaller ones. Outer oral styles composed of two jointed subunits: a rectangular, basal piece with two proximal fringes located at their lateral edges with a couple of tips each one; and a triangular, hooked, distally pointed and curved end-piece (Fig. 6B). Triangular, poorly sclerotized cuticular thickenings flanking the outer oral styles. Outer oral styles located anterior to each introvert sector, except in the middorsal sector 6.

Introvert with six rings of scalids (one ring of primary spinoscalids and five rings of regular-sized scalids) and 10 longitudinal sectors delimited by the arrangement of the primary spinoscalids. Ring 01 of introvert with 10 primary spinoscalids, larger than

remaining ones, laterally compressed, composed of a medially fringed basal sheath and a distal, elongated, flexible, distally pointed end-piece. Remaining rings of introvert with scalids variable in size but always smaller than the primary spinoscalids, morphologically similar to the latter (Fig. 6C). Scalids tend to collapse when mounted for LM, and specimens for SEM with fully everted heads were not available, so details on the scalid arrangement are not provided.

Neck: 16 trapezoidal placids, slightly wider at base, closely adjacent, with distinct joint between the neck and first trunk segment. Midventral placid widest (ca. 13–15μm wide at base), remaining ones narrower (ca. 8–10μm wide at base). A ring of six long, superficially haired trichoscalids associated with the placids, attached to small, rounded trichoscalid plates (Figs. 5A-B; 6C-D; 7A-C; 9A-B).

Trunk: fusiform to softly rectangular, composed of 11 segments, heart-shaped in cross-section. Segments 1–2 closed, ring-like cuticular plates, remaining ones with one tergal and two sternal cuticular plates (Figs. 5A-D; 6A; 9A). Maximum sternal width at segment 8, trunk progressively tapering toward anterior and posterior ends. Cuticular hairs throughout segments 1–10, acicular, non-bracteate, distally pointed, emerging from rounded to slightly oval perforation sites. Cuticular hairs arranged as 8–10 (dorsal) and 4–6 (ventral) straight, irregular, transversal rows densely covering the whole surface of segment 1 dorsally and the most posterior half of the segment ventrally; as 6–8 transversal rows densely covering the whole surface of segment 2; as 6–16 transversal rows, becoming wavy at the lateral and ventral areas, densely covering the whole surface of segments 3–9 except in the vicinity of the droplet-shaped sensory spots and the large, oval areas (muscular scars) in laterodorsal and paraventral positions (also of segment 10 in females); as 3–5 transversal rows densely covering the midlateral to ventrolateral region of segment 10 in males (Figs. 5A-D; 6E-G; 7A-G; 8A-B, G; 9B-L). Muscular scars in laterodorsal position on segments 3–9, with several spherical perforations (Figs. 5A-B; 7A-B, D; 8A; 9B, E, J). Posterior segment margins straight, with a strongly serrated primary pectinate fringe (Figs. 5A-D; 6F-G; 7A-G; 8A-C, E, G; 9A-B, D-F, H-J, L). Secondary pectinate fringes not detected.

Segment 1: type 1 glandular cell outlets in middorsal and lateroventral positions, the former near the anterior segment margin, the latter located at the anterior half of the segment (Figs. 5A-B; 7A-C); type 1 glandular cell outlets on this and following segments rounded, with a single pore. Rounded sensory spots (sensu Lundbye et al. 2011) in

subdorsal, laterodorsal and lateroventral positions (Figs. 5A-B; 7A-C; 9B-C). Rounded sensory spots as circular, depressed areas with 5–6 rings of micropapillae surrounding a single, central pore with a short, emerging cilium (Fig. 9B-C).

Segment 2: droplet-shaped sensory spots (sensu Lundbye et al. 2011) in subdorsal, laterodorsal and ventrolateral positions (Figs. 5A-B; 7A-C; 9B). Droplet-shaped sensory spots, on this and following segments, as oval areas with 7–8 rings of micropapillae with a single, anterior pore from which a long, thin cilium may emerge (Fig. 9B, E-H; J-K).

Segment 3: droplet-shaped sensory spots in subdorsal and midlateral position (Figs. 5B; 7A-C; 9B).

Segment 4: acicular spine in middorsal position (Figs. 5B; 7A-B; 9D); acicular spines on this and following segments are short (ca. 3–8µm long), poorly sclerotized and weakly articulated (Figs. 5A-B; 7E-G; 9D, H-I). Type 2 glandular cell outlets in midlateral position (Fig. 5B; 7C; 9E); type 2 glandular cell outlets, on this and following segments, as minute, circular areas smaller than sensory spots bearing a single pore (Fig. 9E, G-H, J). Droplet-shaped sensory spots in subdorsal position only in males (Figs. 5B; 7A).

Segment 5: tubes in lateroventral position (Figs. 5A; 7E-F; 9E). Type 2 glandular cell outlets in subdorsal position (Figs. 5B; 7D; 9E). Type 1 glandular cell outlets in ventromedial position (Figs. 5A; 7F). Droplet-shaped sensory spots in midlateral and ventromedial positions (Figs. 5A-B; 7D, F; 9E-F).

Segment 6: acicular spines in lateroventral position (Figs. 5A; 7E-F). Type 2 glandular cell outlets in subdorsal and lateral accessory positions (Figs. 5A-B; 7D-F; 9E, G). Type 1 glandular cell outlets in ventromedial position (Figs. 5A; 7F). Droplet-shaped sensory spots in subdorsal, midlateral and ventromedial positions, the former located more lateral than the subdorsal type 2 glandular cell outlets but still in subdorsal position (Figs. 5A-B; 7D, F; 9E-G).

Segment 7: acicular spines in sublateral position (Figs. 5A; 7E; 9H). Type 2 glandular cell outlets in sublateral position, slightly lateral or above the acicular spines (Figs. 5A; 7E; 9H). Type 1 glandular cell outlets in ventromedial position (Fig. 5A). Droplet-shaped sensory spots in subdorsal, midlateral and ventromedial positions (Figs. 5A-B; 9F, H).

Segment 8: acicular spines in lateral accessory position, and large tubes in sublateral position (Figs. 5A; 7E, G; 9I). Type 1 glandular cell outlets in ventromedial position (Figs. 5A; 7G). Droplet-shaped sensory spots in subdorsal and ventromedial positions (Figs. 5A-B; 7G; 8A).

Segment 9: type 2 glandular cell outlets in laterodorsal position (Figs. 5B; 8A; 9J). Type 1 glandular cell outlets in ventromedial position (Figs. 5A; 8B). Droplet-shaped sensory spots in paradorsal, subdorsal, midlateral and ventrolateral positions (Figs. 5A-B; 8A-B; 9J-K). Nephridiopores in sublateral position as triangular, enlarged sieve plates consisting of a slightly convex area with numerous pores followed by a small posterior, slightly concave region with a single, enlarged pore (Figs. 5A-B; 6F-G; 9J).

Segment 10: retractable into segment 9 (Figs. 5A-D; 6A; 9A). Large tubes in laterodorsal position only in males (Figs. 5B; 8E; 9J, L). Two type 1 glandular cell outlets in middorsal position, longitudinally aligned (Figs. 5B, D; 8E). Tergal plate of males with a pair of cuticular extensions in subdorsal position, rectangular, with straight, abruptly tapering, slightly curved tips protruding into the cuticular surface of the following segment; tergal plates of females with tufts of hairs instead (Figs. 5A-B, D; 8E).

Segment 11: retractable into segments 9–10 (Figs. 5A-D; 6A; 9A). Relatively long lateral terminal spines (LTS:TL average ratio = 52.9%), apparently well sclerotized but still flexible, distally pointed, with a hollow central cavity (Figs. 5A-D; 6E; 8D; 9A, L). Males with three pairs of penile spines, dorsal and ventral pairs longer and slender, smooth and distally rounded, medial pair shorter and stouter, hairy and distally blunt (Figs. 5A-B; 8C; 9L); females with short (LTAS:LTS value=10.1%), slender, lateral terminal accessory spines (Figs. 5C-D; 8F). Female gonopores near the anterolateral margins of sternal plates (Fig. 8G). Type 1 glandular cell outlet in middorsal position (Figs. 5B, D; 8E). Tergal plate of males with a middorsal, triangular, bulged process that extends slightly beyond the tergal extensions; blade-like tergal extensions, distally pointed (Figs. 5A-D; 8D-E; 9L). Sternal extensions short, distally rounded (Figs. 5A, C; 8F-G).

3.2.5 Remarks

Several specimens were found with ingested clusters of diatoms in the hindgut (segments 8–10) (Fig. 6H). Interestingly, the diatoms seem to be unaltered despite they were swallowed by the animals.

461

462 *3.3 Statistics*

463 Statistically significant differences in richness (Fig. 10A) and density (Fig. 10B) were not
464 found between the two analysed sites ("impacted" vs. "control"), as indicated by the *p*-
465 values (richness, p=0.3173; density, p=0.8273).

466 The low number of samples prevented us to test the differences in the community
467 species composition statistically (Fig. 10C).

468

469 **4. Discussion**

470 *4.1 Designation of* Echinoderes cyaneafictus *sp. nov. and* E. parthenope *sp.nov. to a*
471 *putative species group*.

472 One of the best supported putative groups within *Echinoderes* is the *E. coulli*-group
473 (Sørensen 2014; Randsø et al. 2019). The group is mainly composed of intertidal,
474 brackish species with enlarged nephridiopores (oval or triangular, convex plate with
475 multiple pores plus a posterior, oval, concave area with a single pore), a feature that
476 supposedly confers an adaptive advantage to cope with extreme salinity fluctuations
477 (Lundbye et al. 2011, Randsø et al. 2019). However, there are some exceptions to this.
478 *Echinoderes regina* Yamasaki, 2016, *E. rex* Lundbye et al., 2011 and *E. serratulus*
479 Yamasaki, 2016 are strictly subtidal (up to 13 m depth), marine species (Lundbye et al.
480 2011; Yamasaki 2016). In addition, there is a still undescribed species from the New
481 Zealand deep-sea (up to 1013m depth) (Sørensen, personal communication). These
482 species unequivocally belong to the group since they possess the enlarged nephridiopore,
483 suggesting its adaptation to salinity fluctuations (Randsø et al. 2019). This *E. coulli*-group
484 is furthermore characterized by sharing the following combination of morphological
485 features: middorsal spines absent or poorly developed on segment 4 only, lateroventral
486 spines absent or poorly developed on segments 6–7 only, female lateral terminal
487 accessory spines absent or poorly developed, and lateral tubes on segments 5 and 8
488 (Sørensen 2014; Randsø et al. 2019). However, as it can be seen, the presence of enlarged
489 nephridiopores remains as the only consistent apomorphy present throughout the group
490 (Randsø et al. 2019).

Echinoderes cyaneafictus sp. nov. seems to fit well within the *E. coulli*-group since it has all the morphological characteristics shared by the members of the group (Randsø et al. 2019). *Echinoderes cyaneafictus* sp. nov. shows closest resemblance to *E. regina*, *E. rex* and *E. serratulus*, of which *E. rex* is part of the Clade C/III (Randsø et al. 2019). The phylogenetic position of *E. regina* still remains problematic, as it is very sensitive to the different inference approaches and choice of molecular markers (Randsø et al. 2019). *Echinoderes regina* was never recovered in the molecular and total-evidence phylogenies together with *E. rex* or *E. serratulus*, and the support value of Clade A (*E. regina* + *E. annae* Sørensen et al., 2016 and *E. serratulus*) in the morphological phylogenies was low (Randsø et al. 2019). On the other hand, *E. serratulus* seems to be more closely related to *E. annae* and *E. hwiizaa* Yamasaki & Fujimoto, 2014 according to both molecular and total-evidence phylogenies (Randsø et al. 2019) and, as above mentioned, its occurrence together with *E. regina* in Clade A in the morphological phylogenies cannot be trusted. Thus, this apparent morphological resemblance of *E. regina, E. rex, E. serratulus* and *E. cyaneafictus* sp. nov. is not indicative of a close relationship.

We also consider *Echinoderes parthenope* sp. nov. part of the *E. coulli*-group since it agrees with the only identified morphological apomorphy: the presence of enlarged nephridiopores composed of an anterior, oval or triangular, convex plate with multiple pores and a posterior, oval, concave area with a single, large pore (Randsø et al. 2019). Actually, the shape of its nephridiopores, as a triangle instead of an oval area, resembles that of *E. maxwelli* Omer-Cooper, 1957 and *E. komatsui* (Lundbye et al. 2011; Yamasaki & Fujimoto 2014). However, Randsø et al. (2019) did not find support for a homology between the triangular sieve plates.

4.2 Remarks on diagnostic and differential taxonomic features of Echinoderes cyaneafictus *sp. nov. and* Echinoderes parthenope *sp.nov.*

The *Echinoderes coulli*-group currently comprises 13 species: *E. annae*, *E. applicitus*, *E. coulli* Higgins, 1977, *E. hwiizaa*, *E. komatsui*, *E. marthae* Sørensen, 2014, *E. maxwelli*, *E. ohtsukai* Yamasaki & Kajihara, 2012, *E. regina*, *E. rex*, *E. serratulus*, *E. strii*, and *E. teretis* (Randsø et al. 2019). Furthermore, *E. aspinosus* Sørensen et al., 2012, *E.*

522 *bengalensis*, and *E. caribiensis* could also be part of the group, although the presence of
523 the characteristic sieve plate needs to be confirmed (Randsø et al. 2019).

524 *Echinoderes cyaneafictus* sp. nov. shares a similar spine and tube pattern with *E.*
525 *maxwelli*, *E. regina* and *E. serratulus*, with slight differences. Spines of segment 6 are in
526 lateroventral position in *E. maxwelli* (sublateral in the new species), and tubes of segment
527 8 are in sublateral position in *E. regina* and lateroventral position in *E. serratulus* (lateral
528 accessory in the new species) (Yamasaki 2016; Randsø et al. 2019). Furthermore, *E.*
529 *serratulus* possesses tubes in midlateral position on segment 9 (Yamasaki 2016), which
530 are absent in *E. cyaneafictus* sp. nov. The three congeners may also be distinguished from
531 the new species by the presence of minute type 2 glandular cell outlets throughout
532 segments 1–8 (Yamasaki 2016; Randsø et al. 2019), structures otherwise missing in *E.*
533 *cyaneafictus* sp. nov. Finally, the new species is characterized by three pairs of large,
534 rounded sensory spots on segment 1 with a traversal row of conspicuously elongated hairs
535 at the posterior part of the papillae area. Although the other three species also have
536 sensory spots on segment 1, they are morphologically different and lack the significant,
537 posterior row of elongated hairs. These sensory spots have been observed in the same
538 positions of segment 1 of another still undescribed congener of the *E. coulli*-group with
539 scanning electron microscopy (Cepeda et al. unpublished). *Echinoderes cyaneafictus* sp.
540 nov. may be distinguished from this other congener by the absence of type 2 glandular
541 cell outlets, apart from other minor differences concerning the sensory spot arrangement
542 (Cepeda et al. unpublished).

543 *Echinoderes parthenope* sp. nov. is unique within the *E. coulli*-group due to the
544 presence of spines on segment 8. Only *E. caribiensis* was originally described with
545 lateroventral spines on this segment (Kirsteuer 1964), but the description of this species
546 is quite incomplete, type material is missing and it has been never found again (despite
547 the multiple taxonomic efforts done at the Caribbean area, e.g. Higgins 1983; Sørensen
548 2006; Pardos et al. 2016b; Cepeda et al. 2019a; 2019c). Thus, we can question the actual
549 validity of the morphological data concerning *E. caribiensis*. Members of the *E. coulli*-
550 group may have spines in middorsal position on segment 4 and in lateral position on
551 segments 6–7, but these spines are conspicuously small, poorly sclerotized and weakly
552 articulated. In contrast, tubes, which may be present at different positions throughout the
553 trunk, are large and well developed (Sørensen 2014; Randsø et al. 2019). Thus, the
554 lateroventral spines on segments 8–9 of *E. caribiensis* could be actually tubes, as they

were described and illustrated as large, conspicuous, well sclerotized cuticular appendages (Kirsteuer 1964). Nevertheless, the spine and tube pattern of *E. caribiensis* is completely different from that of *E. parthenope* sp. nov., including the absence of middorsal spine and lateral spines on segments 6–7 (Kirsteuer 1964), structures otherwise present in the new species. The characteristic triangular sieve plate of *E. parthenope* sp. nov. is also found in *E. komatsui* and *E. maxwelli*, but both congeners may be easily distinguished from the new species. *Echinoderes komatsui* lacks a middorsal spine on segment 4 and lateral spines on segments 6–7 (Yamasaki & Fujimoto 2014), which are present in *E. parthenope* sp. nov. *Echinoderes maxwelli* also lacks spines on segment 8, having tubes instead in lateral accessory position (Omer-Cooper 1957; Randsø et al. 2019) (*E. parthenope* with lateral accessory spines and sublateral tubes on this segment), but otherwise is quite similar to the new species in terms of spine and tube arrangement. However, both species differ in the type 2 glandular cell outlet arrangement as well as some sexually dimorphic features, including the presence of laterodorsal tubes on segment 10 only in males in *E. parthenope* sp. nov. (both sexes in *E. maxwelli*) and the shape of the male tergal plate of segment 11 (Randsø et al. 2011), which is unique of the new species.

4.3 Biogeographic remarks.

By considering the two new species as part of the *E. coulli*-group, some interesting biogeographic data may be taken into account.

Randsø et al. (2019) proposed some phylogeographic hypotheses about the current distribution of the *E. coulli*-group members, pointing out to a scenario of vicariance between the New World and the Old World representatives, with the latter being present in a vast shallow-water sea of the southern palaeo-Tethys Ocean by mid-late Silurian (ca. 426–416ma ago) (Metcalfe 2006; Randsø et al. 2019; Liu et al. 2021). However, the current distribution of *E. maxwelli* (South Africa), one of the Old World representatives, does not fit this hypothesis (Randsø et al. 2019). If we consider *E. cyaneafictus* sp. nov. and *E. parthenope* sp. nov. as part of the *E. coulli*-group, with their current known distribution in Mayotte, we have another case that does not fit the hypothesis of Randsø et al. (2019).

Of course, this scenario would only be possible with a high rate of morphological conservation after speciation, as proposed by Randsø et al. (2019), but the hypothesis of having a rather recent speciation of the *E. coulli*-group members cannot be completely disregarded, especially after the discovering of *E. cyaneafictus* sp. nov. and *E. parthenope* sp. nov.

4.4 Ecological considerations

In a previous study of the same area (Capdeville et al. 2018), Kinorhyncha was found as one of the most abundant meiofaunal taxa in the mangrove forest, only surpassed by nematodes, copepods, foraminiferans and tanaidaceans. Although Capdeville et al. (2018) did not measure any effect of the wastewater discharge on the total meiofauna abundance, nor on the abundance of the main meiofaunal groups, they found that kinorhynch abundance significantly decreased in the "impacted" plot. These results, however, were not recovered in the present study, as both richness and density seem not to be affected by sewage inputs. We might explain such differences between our results and those of Capdeville et al. (2018) by the fact that the wastewater discharge experiments were stopped right before our sampling, leaving time to the mangrove ecosystem to slowly recover.

Although there was no significant differences in the density neither richness of kinorhynchs, *E. parthenope* sp. nov. seems to be less sensitive to pollutants from wastewater, being able to maintain stable communities in the "impacted" area. Only a single specimen of *E. parthenope* sp. nov. was found at the "control" site. Contrarily, *E. cyaneafictus* sp. nov. was only found in the "control" area.

Meiofauna is known to be extremely sensitive to pollution and environmental changes (Giere 2009). Specifically, meiofaunal organisms strongly rely on sediment properties, especially particle size, available oxygen, pH and organic matter content (Nagelkerken et al. 2008; Giere 2009). Several studies verified that Kinorhyncha density is negatively impacted when the amount of organic matter strongly increases due to domestic sewage or aquatic farms (e.g. Santos et al. 2009; Capdeville et al. 2018; Carugati et al. 2018). The increase of organic matter content may initially enhance microbial proliferation (bacteria and microalgae), one of the likely food sources for kinorhynchs, which could be beneficial for these animals (Nomaki et al. 2008; Bouchez et al. 2013;

Capdeville et al. 2018). However, it also causes a decrease in the available oxygen and stimulates the formation of hydrogen sulfide, which may explain the negative long-term impact (Ansari et al. 1984; Sutherland et al. 2007; Dal Zotto et al. 2016; Capdeville et al. 2018).

In our study, Kinorhyncha density was not affected by sewage discharge, which resembles the results of De Paula et al. (2006), who even observed an increase in kinorhynch abundance due to an input of organic matter from an aquatic farm. Indeed, one of the species, *Echinoderes parthenope* sp. nov., mostly appeared in the "impacted" site. This could be because, initially, when the input of organic matter is not very high and therefore the dissolved oxygen is not excessively compromised or the sulfide concentrations are still low, the abundance of kinorhynchs may be enhanced due to a greater availability of resources (Pearson & Rosenberg 1978; Reish 1980; Dal Zotto et al. 2016). Another reason could be that Kinorhyncha of the studied mangrove (at least *E. parthenope* sp. nov.) are opportunistic, more specialized species able to cope with the wastewater influence and even profiting about this. This hypothesis has been previously applied in similar situations of extreme or polluted environmental conditions to explain the boost of some meiofaunal densities, including those of Kinorhyncha (Ritt et al. 2010; Vanreusel et al. 2010; Cepeda et al. 2020; Sánchez et al. 2021). The apparent absence of *E. cyaneafictus* sp. nov. at the "impacted" site does not have to be necessarily correlated with a negative effect of wastewater, but simply with the higher prevalence of the other species, *E. parthenope* sp. nov., giving rise to a process of interspecific competition. A third scenario could be the absence of sufficient environmental discrepancies among the studied sites ("impacted" vs. "control"). However, this option is the most unlikely, as previous studies showed great physico-chemical differences in the same places despite their closeness (Bouchez et al. 2013; Capdeville et al. 2018, 2019).

In general terms, a moderate impact due to wastewater discharge from a small population in a mangrove swamp should not necessarily mean a major dysfunction of the ecosystem, at least during a limited period of time (Capdeville et al. 2018). Mangroves seem to be both resistant and resilient ecosystems, absorbing nutrients in excess from sewage without major structural or functional disturbances (Saenger 2002; Capdeville et al. 2018, 2019), at least under the conditions previously mentioned. The spatial-temporal scale at which the studies are carried out is also vital when analyzing the levels of deterioration of an ecosystem. Thus, the results may differ from general studies of the

benthic fauna to those that identify individuals at lower taxonomic levels (Michelet et al. 2021). Nevertheless, hydrodynamics of the area, sediment properties and specific biological characteristics are key to define the efficiency of a mangrove ecosystem in sewage treatment and must be always taken into account (Clough et al. 1983). Under this scenario, with the present evidence, we cannot either confirm or reject a negative effect of domestic sewage on the Kinorhyncha community inhabiting the studied mangrove area. Further samplings with quantitative ecological data would be needed in order to clarify the situation in the future.

Declaration of competing interest

The authors declare that they have not known competing financial interests or personal relationships that could have appeared to influence the work reported in this paper.

Acknowledgements

The authors would like to express their gratitude to Fernando Pardos (UCM) for providing the facilities as well as the equipment and material of light microscopy that were necessary for the present study, as well as for their invaluable advices while writing the manuscript. Mayotte fieldwork was done by the French working group "Mangroves DCE" under the framework of the European Water Framework Directive (G. Dirberg, C. Hubas, P. Cuny, C. Militon, R. Walcker, F. Fromard, I. Bihannic, E. Michaud) in collaboration with the Water Syndicate of Mayotte (SIEAM) (K. Abdullah). The authors are also grateful to University Center of Mayotte (CUFR) for providing the corresponding facilities and to Claire Michelet for helping with the meiofaunal sorting. This project was funded by Office Français de la Biodiversité (OFB).

References

Adrianov, A.V., Malakhov, V.V., 1999. Cephalorhyncha of the World Ocean, first ed. KMK Scientific Press, Moscow.

679 Alongi, D.M., 1987. The influence of mangrove-derived tannins on intertidal
680 meiobenthos in tropical estuaries. Oecologia 71, 537–540. https://doi.org/
681 10.1007/BF00379293.

682 Alongi, D.M., 1990. Abundances of benthic microfauna in relation to outwelling of
683 mangrove detritus in a tropical coastal region. Mar. Ecol. Prog. Ser. 63, 53–63.
684 https://doi.org/ 10.3354/meps063053.

685 Alongi, D.M., 2002. Present state and future of the world's mangrove forests. Environ.
686 Conserv. 29, 331–349. https://doi.org/10.1017/S0376892902000231

687 Annapurna, C., Rao, M.S., Bhanu, C.H.V., 2015. Distribution of meiobenthos off
688 Kakinada Bay, Gaderu and Coringa estuarine complex. J. Mar. Biol. Assoc. India 57, 17–
689 26.

690 Ansari, Z.A., Chatterji, A., Parulekar, A.H., 1984. Effect of domestic sewage on sand
691 beach meiofauna at Goa, India. Hydrobiologia 111, 229–233.
692 https://doi.org/10.1007/BF00007203.

693 Bartolini, F., Cimò, F., Fusi, M., Dahdouh-Guebas, F., Lopes, G.P., Cannicci, S., 2011.
694 The effect of seawage discharge on the ecosystem engineering activities of two East
695 African fiddler crab species: consequences for mangrove ecosystem functioning. Mar.
696 Environ. Res. 71, 53–61. https://doi.org/ 10.1016/j.marenvres.2010.10.002.

697 Bouchez, A., Pascault, N., Chardon, C., Bouvy, M., Cecchi, P., Lambs, L., Herteman, M.,
698 Fromard, F., Got, P., Leboulanger, C., 2013. Mangrove microbial diversity and the impact
699 of trophic contamination. Mar. Pollut. Bull. 66, 39–46.
700 https://doi.org/10.1016/j.marpolbul.2012.11.015.

701 Capdeville, C., Abdallah, K., Buffan-Dubau, E., Lin, C., Azemar, F., Lambs, L., Fromard,
702 F., Rols, J.L., Leflaive, J., 2018. Limited impact of several years of pretreated wastewater
703 discharge on fauna and vegetation in a mangrove ecosystem. Mar. Pollut. Bull. 129, 379–
704 391. https://doi.org/10.1016/j.marpolbul.2018.02.035.

705 Capdeville, C., Pommier, T., Gervaix, J., Fromard, F., Rols, J.L., Leflaive, J., 2019.
706 Mangrove facies drives resistance and resilience of sediment microbes exposed to
707 anthropic disturbance. Front. Microbiol. 15, e3337.
708 https://doi.org/10.3389/fmicb.2018.03337.

Carugati, L., Gatto, B., Rastelli, E., Lo Martire, M., Coral, C., Greco, S., Danovaro, R., 2018. Impact of mangrove forests degradation on biodiversity and ecosystem functioning. Sci. Rep. 8, e13298. https://doi.org/10.1038/s41598-018-31683-0.

Carus, J. V., 1885. Prodromus Faunae Mediterraneae sive Descriptio Animalium maris Mediterranei incolarum quam comparata silva rerum quatenus innotiut adiectis et nominibus vulgaribus eorumque auctoribus in commodum zoologorum. Vol. I. Coelenterata, Echinodermata, Vermes, Arthropoda, first ed. E. Schweizerbartsche Verlagshandlung E. Koch, Stuttgart.

Cepeda, D., 2021. Further Steps in Systematics, Biology and Ecology of the Phylum Kinorhyncha, Ph.D. Dissertation. Universidad Complutense de Madrid, Madrid.

Cepeda, D., Pardos, F., Sánchez, N., 2019a. A new species and first record of *Dracoderes* (Kinorhyncha: Allomalorhagida: Dracoderidae) from American waters, with an identification key of the genus. Zool. Anz. 282, 106–115. https://doi.org/10.1016/j.jcz.2019.05.019.

Cepeda, D., Pardos, F., Sánchez, N., 2019b. Kinorhyncha from the Caribbean, with the description of two new species from Puerto Rico and Barbados. Zool. Anz. 282, 127–139. https://doi.org/10.1016/j.jcz.2019.05.014.

Cepeda, D., Pardos, F., Zeppilli, D., Sánchez, N., 2020. Dragons of the deep sea: Kinorhyncha communities in a pockmark field at Mozambique Channel, with the description of three new species. Front. Mar. Sci. 7, e665. http://doi.org/10.3389/fmars.2020.00665.

Cepeda, D., Sánchez, N., Gayet, N., Spedicato, A., Michaud, E., Zeppilli, D., this issue. Description of two new species of *Echinoderes* Claparède, 1863 (Kinorhyncha: Cyclorhagida: Echinoderidae) from a polluted mangrove swamp in French Guiana (western Atlantic Ocean). Zool. Anz. this issue.

Cepeda, D., Sánchez, N., Pardos, F., 2019c. First extensive account of the phylum Kinorhyncha from Haiti and the Dominican Republic (Caribbean Sea), with the description of four new species. Mar. Biodivers. 49, 2281–2309. https://doi.org/10.1007/s12526-019-00963-x.

738 Claparède, A.R.É., 1863. Beobachtungen über Anatomie und Entwicklungsgeschichte
739 wirbelloser Thiere: an der Küste von Normandie angestellt, first ed. Verlag von Wilhelm
740 Engelmann, Leipzig.

741 Clough, B.F., Boto, K.G., Attiwill, P.M., 1983. Mangroves and sewage – a re-evaluation.
742 In: Thas, H.J. (Ed.), Biology and Ecology of Mangroves. Tasks for Vegetation Science,
743 Vol. 8. Springer, Dordrecht, The Netherlands, pp. 151–161. https://doi.org/10.1007/978-
744 94-017-0914-9_17.

745 Coull, B.C., 1988. Ecology of the marine meiofauna. In: Higgins, R.P., Thiel, H. (Eds.),
746 Introduction to the Study of Meiofauna. Smithsonian Institution Press, Washington D.C.,
747 U.S.A., pp. 18–38.

748 Dal Zotto, M., Santulli, A., Simonini, R., Todaro, M.A., 2016. Organic enrichment effects
749 on a marine meiofauna community, with focus on Kinorhyncha. Zool. Anz. 265, 127–
750 140. https://doi.org/10.1016/j.jcz.2016.03.013.

751 De Paula, J.H.C., Rosa-Filho, J.S., De Souza, A.L.B., Aviz, D., 2006. A meiofauna como
752 indicadora de impactos de carcinicultura no estuario de Curuça (PA). Boletim do
753 Laboratório de Hidrobiologia 19, 61–72.

754 Della Patrona, L.; Marchand, C.; Hubas, C.; Molnar, N.; Deborde, J.; Meziane, T., 2016.
755 Meiofauna distribution in a mangrove forest exposed to shrimp farm effluents (New
756 Caledonia). Mar. Environ. Res. 119, 100–113. https://doi.org/
757 10.1016/j.marenvres.2016.05.028.

758 Duke, N.C., 2016. Oil spill impacts on mangroves: recommendations for operational
759 planning and action based on a global review. Mar. Pollut. Bull. 109, 700–715.
760 https://doi.org/10.1016/j.marpolbul.2016.06.082.

761 Edgar G., 1990. The influence of plant structure on the species richness, biomass and
762 secondary production of macrofaunal assemblages associated with Western Australian
763 seagrass beds. J. Exp. Mar. Biol. Ecol. 137, 215–240.

764 Fonseca, V. G., Carvalho, G. R., Sung, W., Johnson, H. F., Power, D. M., Neill, S. P.,
765 Packer, M., Blaxter, M. L., Lambshead, P. J., Thomas, W. K., Creer, S., 2010. Second-
766 generation environmental sequencing unmasks marine metazoan biodiversity. Nat.
767 Commun. 1, 98. https://doi.org/10.1038/ncomms1095.

768 Giere, O., 2009. Meiobenthology: The Microscopic Motile Fauna of Aquatic Sediments,
769 first ed. Springer Science & Business Media Springer-Verlag, Berlin Heidelberg.

770 Gilman, E.L., Ellison, J., Duke, N.C., Field, C., 2008. Threats to mangroves from climate
771 change and adaptation options: a review. Aquat. Bot. 89, 237–250.
772 https://doi.org/10.1016/j.aquabot.2007.12.009.

773 Gomes C. A. A., Dos Santos, P. J. P., Alves, T. N. C., Rosa-Filho, J. S., Souza-Santos, L.
774 P., 2002. Variaçao temporal da meiofauna em Area de Manguezal em Itamaraca –
775 Pernambuco. Atlântica, Rio Grande 24, 89–96.

776 Heip, C.H.R., Vincx, M., Vranken, G., 1985. The ecology of marine nematodes.
777 Oceanogr. Mar. Biol. 23, 399–489.

778 Herranz, M., Stiller, J., Worsaae, K., Sørensen, M.V., 2022. Phylogenomic analyses of
779 mud dragons (Kinorhyncha). Mol. Phylogenet. Evol. 168, 107375.
780 https://doi.org/10.1016/j.ympev.2021.107375.

781 Herteman, M., Fromard, F., Lambs, L., 2011. Effects of pretreated domestic wastewater
782 supplies on leaf pigment content, photosynthesis rate and growth of mangrove trees: a
783 field study from Mayotte Island, SW Indian Ocean. Ecol. Eng. 37, 1283–1291.
784 https://doi.org/10.1016/j.ecoleng.2011.03.027.

785 Higgins, R.P., 1969. Indian Ocean Kinorhyncha: 1. *Condyloderes* and *Sphenoderes*, new
786 cyclorhagid genera. Smithsonian Contrib. Zool. 14, 1–13.
787 https://doi.org/10.5479/si.00810282.14.

788 Higgins, R.P., 1977. Two new species of *Echinoderes* (Kinorhyncha) from South
789 Carolina. Trans. Am. Microsc. Soc. 96, 340–354. https://doi.org/10.2307/3225864.

790 Higgins, R.P., 1983. The Atlantic barrier reef ecosystem at Carrie Bow Cay, Belize, II.
791 Kinorhyncha. Smithsonian Contrib. Mar. Sci. 18, 1–131.
792 https://doi.org/10.5479/si.01960768.18.1.

793 Hodda, M., Nicholas, W. L., 1986. Temporal changes in littoral meiofauna from the
794 Hunter River estuary. Aust. J. Mar. Freshw. Res. 37, 729–741.

795 Hogarth, P.J., 1999. The Biology of Mangroves, first ed. Oxford University Press,
796 Oxford.

Kathiresan, K., Bingham, B. L., 2001 Biology of mangroves and mangrove ecosystems. Adv. Mar. Biol. 40, 81–251. https://doi.org/ 10.1016/S0065-2881(01)40003-4.

Khalil, A.S.M., 2019. 23. Meiofauna of the Red Sea mangroves with emphasis on their response to habitat degradation: Sudan's mangroves as a case study. In: Rasul, N.M.A., Stewart I.C.F. (Eds.), Oceanographic and Biological Aspects of the Red Sea. Springer International Publishing, New York, U.S.A., pp. 419–435. https://doi.org/ 10.1007/978-3-319-99417-8_23.

Kirsteuer, E., 1964. Zur Kenntnis der Kinorhynchen Venezuelas. Zool. Anz. 173, 388–393.

Lewis, M., Pryor, R., Wilking, L., 2011. Fate and effects of anthropogenic chemicals in mangrove ecosystems: a review. Environ. Pollut. 159, 2328–2346. https://doi.org/10.1016/j.envpol.2011.04.027.

Liu, J., Chen, X., Fan, W., Shan, H., Yan, J., Ding, X., Zhao, T., Yu, X., Liu, Z., Xu, Z., 2021. Dynamics of closure of the Proto-Tethys Ocean: a perspective from the Southeast Asian Tethys realm. Earth-Sci. Rev. 222, e103829. https://doi.org/10.1016/j.earscirev.2021.103829.

Lundbye, H., Rho, H.S., Sørensen, M.V., 2011. *Echinoderes rex* n. sp. (Kinorhyncha: Cyclorhagida), the largest *Echinoderes* species found so far. Sci. Mar. 75, 41–51. https://doi.org/10.3989/scimar.2011.75n1041.

Metcalfe, I., 2006. Palaeozoic and Mesozoic tectonic evolution and palaeogeography of East Asian crustal fragments: the Korean Peninsula in context. Gondwana Res. 9, 24–46. https://doi.org/10.1016/j.gr.2005.04.002.

Michelet, C., Zeppilli, D., Hubas, C., Baldrighi, E., Cuny, P., Dirberg, G., Militon, C., Walcker, R., Lamy, D., Jezequel, R., Receveur, J., Gilbert, F., El Houssainy, A., Dufour, A., Heimbürger-Boavida L. E., Bihannic, I. Sylvi, L., Vivier, B., Michaud, E., 2021. First assessment of the benthic meiofauna sensitivity to low human-impacted mangroves in French Guiana. Forests 12, 338. https://doi.org/10.3390/f12030338.

Mokievsky, V.O., Tchesunov, A.V., Udalov, A.A., Duy-Toan, N., 2011. Quantitative distribution of meiobenthos and the structure of the free-living nematode community of the mangrove intertidal zone in Nha Trang Bay (Vietnam) in the South China Sea. Russ. J. Mar. Biol. 37, 272–283. https://doi.org/10.1134/S1063074011040109.

828 Molnar, N., Welsh, D.T., Marchand, C., Deborde, J., Meziane, T., 2013. Impacts of
829 shrimp farm effluent on water quality, benthic metabolism and N-dynamics in a
830 mangrove forest (New Caledonia). Estuar. Coast. Shelf Sci. 117, 12–21.
831 https://doi.org/10.1016/j.ecss.2012.07.012.

832 Nagelkerken, I., Blaber, S.J.M., Bouillon, S., Green, P., Haywood, M., Kirton, L.G.,
833 Meynecke, J.O., Pawlik, J., Penrose, H.M., Sasekumar, A., Somerfield, P.J., 2008. The
834 habitat function of mangroves for terrestrial and marine fauna: a review. Aquat. Bot. 89,
835 155–185. https://doi.org/10.1016/j.aquabot.2007.12.007.

836 Neuhaus, B., Pardos, F., Sørensen, M.V., Higgins, R.P., 2014. New species of
837 *Centroderes* (Kinorhyncha: Cyclorhagida) from the Northwest Atlantic Ocean, life cycle,
838 and ground pattern of the genus. Zootaxa 3901, 1–69.
839 https://doi.org/10.11646/zootaxa.3901.1.1.

840 Nomaki, H., Ogawa, N.O., Ohkouchi, N., Suga, H., Toyofuku, T., Shimanaga, M.,
841 Nakatsuka, T., Kitazato, H., 2008. Benthic foraminifera as trophic links between
842 phytodetritus and benthic metazoans: carbon and nitrogen isotopic evidence. Mar. Ecol.
843 Prog. Ser. 357, 153–164. https://doi.org/10.3354/meps07309.

844 Ostmann, O., Nordhaus, I., Sørensen, M.V., 2012. First recording of kinorhynchs from
845 Java, with the description of a new brackish water species from a mangrove-fringed
846 lagoon. Mar. Biodivers. 42, 79–91. https://doi.org/ 10.1007/s12526-011-0094-z.

847 Pardos, F., Herranz, M., Sánchez, N., 2016a. Two sides of a coin: the phylum
848 Kinorhyncha in Panama. II) Pacific Panama. Zool. Anz. 265, 26–47.
849 https://doi.org/10.1016/j.jcz.2016.06.006.

850 Pardos, F., Sánchez, N., Herranz, M., 2016b. Two sides of a coin: The phylum
851 Kinorhyncha in Panama. I) Caribbean Panama. Zool. Anz. 265, 3–25.
852 https://doi.org/10.1016/j.jcz.2016.06.005.

853 Pearson, T.H., Rosenberg, R., 1978. Macrobenthic succession in relation to organic
854 enrichment and pollution of the marine environment. Oceanogr. Mar. Biol. 16, 229–311.

855 R Core Team, 2021. R: A language and environment for statistical computing. R
856 Foundation for Statistical Computing, Vienna. https://www.R-project.org/.

Randsø, P.V., Yamasaki, H., Bownes, S.J., Herranz, H., Di Domenico, M., Qii, G.B., Sørensen, M.V., 2019. Phylogeny of the *Echinoderes coulli*-group (Kinorhyncha: Cyclorhagida: Echinoderidae) – a cosmopolitan species group trapped in the intertidal. Invertebr. Syst. 33, 501–517. https://doi.org/10.1071/IS18069.

Reish, D.J., 1980. Effect of domestic wastes on the benthic marine communities of Southern California. Helgolander Meeresun. 33, 377–383. https://doi.org/10.1007/BF02414762.

Ritt, B., Sarrazin, J., Caprais, J.C., Noël, P., Gauthier, O., Pierre, C., Henry, P., Desbruyeres, D., 2010. First insights into the structure and environmental setting of cold-seep communities in the Marmara Sea. Deep-Sea Res. I: Oceanogr. Res. Pap. 57, 1120–1136. https://doi.org/10.1016/j.dsr.2010.05.011.

Saenger, P., 2002. Mangrove Ecology, Silviculture and Conservation, first ed. Kluwer Academic Publishers, Dordrecht.

Sánchez, N., Zeppilli, D., Baldrighi, E., Vanreusel, A., Gasimandova-Lahitsiresy, M., Brandily, C., Pastor, L., Macheriotou, L., García-Gómez, G., Dupré, S., Olu, K., 2021. A threefold perspective on the role of a pockmark in benthic faunal communities and biodiversity patterns. Deep-Sea Res. I: Oceanogr. Res. Pap. 167, e103425. https://doi.org/10.1016/j.dsr.2020.103425.

Santos, P.J.P., Botter-Carvalho, M., Do Nascimento-Junior, A.B., Marinho, R.G.C., Carvalho, P.V.V.C., & Valebça, A.P.M.C., 2009. Response of estuarine maiofauna assemblage to effects of fertilizer enrichment used in the sugar cane monoculture. Pernambuco, Brazil. Braz. J. Oceanogr. 57, 43–55. https://doi.org/ 10.1590/S1679-87592009000100005.

Sasekumar A., Chong V.C., 1998. Faunal diversity in Malaysian mangroves. *Glob. Ecol. Biogeogr. Letters* 7, 57–60. https://doi.org/ 10.1111/J.1466-8238.1998.00279.X.

Schrijvers, J., Schallier, R., Silence, J., Okondo, J. P., Vincx, M., 1997. Interactions between epibenthos and meiobenthos in a high intertidal *Avicennia marina* mangrove forest. Mangrove Salt Marshes 1, 137–154. https://doi.org/10.1023/A:1009936318721.

Somerfield, P.J., Gee, J.M., Aryuthaka, C., 1998. Meiofaunal communities in a Malaysian mangrove forest. J. Mar. Biol. Assoc. U.K. 78, 717–732. https://doi.org/10.1017/S0025315400044738.

888 Sørensen, M.V., 2006. New kinorhynchs from Panama, with a discussion of some
889 phylogentically significant cuticular structures. Meiofauna Marina 15, 51–77.

890 Sørensen, M.V., 2014. First account of echinoderid kinorhynchs from Brazil, with the
891 description of three new species. Mar. Biodivers. 44, 251–274.
892 https://doi.org/10.1007/s12526-013-0181-4.

893 Sørensen, M.V., Dal Zotto, M., Rho, H.S., Herranz, M., Sánchez, N., Pardos, F.,
894 Yamasaki, H., 2015. Phylogeny of Kinorhyncha base on morphology and two molecular
895 loci. PLoS ONE 10, e0133440. https://doi.org/10.1371/journal.pone.0133440.

896 Sørensen, M.V., Gasiorowski, L., Randsø, P.V., Sánchez, N., Neves, R.C., 2016. First
897 report of kinorhynchs from Singapore, with the description of three new species. Raffles
898 Bull. Zool. 64, 3–27. http://doi.org/10.5281/zenodo.4502533.

899 Sukardjo, S., 1994. Soils in the mangrove forests of the Apar Nature Reserve, Tanah
900 Grogot, East Kalimantan, Indonesia. J. Southeast Asian Stud. 32, 385–398.

901 Sutherland, T.F., Levings, C.D., Petersen, S.A., Poon, P., Piercey, B., 2007. The use of
902 meiofauna as an indicator of benthic organic enrichment associated with salmonid
903 aquaculture. Mar. Pollut. Bull. 54, 1249–1261.
904 https://doi.org/10.1016/j.marpolbul.2007.03.024.

905 Timm, R.W., 1958. Two new species of *Echinoderella* (phylum Kinorhyncha) from the
906 Bay of Bengal. J. Bombay Nat. Hist. Soc. 55, 107–109.

907 Uozumi, R., Yamasaki, H., Hirose, E., 2018. Mangrove forests may serve as stable
908 environments for the meiobenthic *Echinoderes komatsui* (Kinorhyncha: Cyclorhagida):
909 distribution patterns and population dynamics in a subtropical estuary. Mar. Biol. Res.
910 14, 321–333. https://doi.org/10.1080/17451000.2017.1408916.

911 Vanreusel, A., De Groote, A., Gollner, S., Bright, M., 2010. Ecology and biogeography
912 of free-living nematodes associated with chemosynthetic environments in the deep-sea: a
913 review. PLoS ONE 5, e12449. https://doi.org/10.1371/journal.pone.0012449.

914 Xie, D., Schwarz, C., Brückner, M.Z.M., Kleinhans, M.G., Urrego, D.H., Zhou, Z., van
915 Maanen, B., 2020. Mangrove diversity loss under sea-level rise triggered by bio-
916 morphodynamic feedbacks and anthropogenic pressures. Environ. Res. Lett. 15, 114033.
917 https://doi.org/10.1088/1748-9326/abc122.

Yamasaki, H., 2016. Two new *Echinoderes* species (Echinoderidae, Cyclorhagida, Kinorhyncha) from Nha Trang, Vietnam. Zool. Stud. 55, 1–35. https://doi.org/10.6620/ZS.2016.55-32.

Yamasaki, H., Fujimoto, S., 2014. Two new species in the *Echinoderes coulli* group (Echinoderidae, Cyclorhagida, Kinorhyncha) from the Ryukyu Islands, Japan. ZooKeys 382, 27–52. https://doi.org/10.3897/zookeys.382.6761.

Yamasaki, H., Kajihara, H., 2012. A new brackish-water species of *Echinoderes* (Kinorhyncha: Cyclorhagida) from the Seto Inland Sea, Japan. Species Divers. 17, 109–118. https://doi.org/10.12782/sd.17.1.109.

Zelinka, C., 1896. Demonstration der Tafeln der *Echinoderes* - Monographie. Verh. Dtsch. Zool. Ges. 6, 197–199.

Zeppilli, D., Leduc, D., Fotanier, C., Fontaneto, D., Fuchs, S., Gooday, A. J., Goineau, A., Ingels, J., Ivanenko, V. N., Kristensen, R. M., Neves, R. C., Sanchez, N., Sandulli, R., Sarrazin, J., Sørensen, M. V., Tasiemski, A., Vanreusel, A., Autret, M., Bourdonnay, L., Claireaux, M., Coquille, V., De Wever, L., Rachel, D., Marchant, J., Toomey, L., Fernandes, D., 2016. Characteristics of meiofauna in extreme marine ecosystems: a review. Mar. Biodivers. 48, 35–71. https://doi.org/10.1007/s12526-017-0815-z.

Zhang, Z.W., Xu, X.R., Sun, Y.X., Yu, S., Chen, Y.S., Peng, J.X., 2014. Heavy metals and organic contaminants in mangrove ecosystems of China: a review. Environ. Sci. Pollut. Res. 21, 11938–11950. https://doi.org/10.1007/s11356-014-3100-8.

946 **TABLES.**

947 **Table 1**. Checklist of mangrove-inhabiting Kinorhyncha prior to this study, including the
948 localities where these species where found living at mangrove areas and the
949 corresponding references.

Species	Ocean	Locality	Reference(s)
Centroderes barbanigra Neuhaus et al., 2014	Western Atlantic	Icaquitos Bay, Dominican Republic	Neuhaus et al. 2014
Cristaphyes belizensis (Higgins, 1983)	Western Atlantic	Carrie Bow Cay, Belize	Higgins 1983
Cristaphyes cornifrons Cepeda et al., 2019	Western Atlantic	La Parguera, Puerto Rico	Cepeda et al. 2019c Cepeda 2021
Cristaphyes longicornis (Higgins, 1983)	Western Atlantic	Carrie Bow Cay, Belize. Puerto Blanco, Dominican Republic.	Higgins 1983 Cepeda et al. 2019a Cepeda 2021
Cristaphyes panamensis Pardos et al., 2016	Western Atlantic	Bastimentos Island, Panama	Pardos et al. 2016b
Cristaphyes retractilis Cepeda et al., 2019	Western Atlantic	La Parguera, Puerto Rico	Cepeda 2021
Dracoderes spyro Cepeda et al., 2019	Western Atlantic	Puerto Príncipe, Haiti. Puerto Blanco, Dominican Republic.	Cepeda et al. 2019b Cepeda 2021
Echinoderes abbreviatus Higgins, 1983	Western Atlantic	Carrie Bow Cay, Belize	Higgins 1983
Echinoderes applicitus Ostmann et al., 2012	Indian	Java, Indonesia	Ostmann et al. 2012
Echinoderes astridae Sørensen, 2014	Western Atlantic	Guantánamo Bay, Cuba. Puerto Príncipe, Haiti. Puerto Blanco, Dominican Republic.	Cepeda et al. 2019a Cepeda 2021
Echinoderes belenae Pardos et al., 2016	Eastern Pacific	Pedro González Island, Panama	Pardos et al. 2016a
Echinoderes bengalensis (Timm, 1958)	Indian	Bay of Bengal	Timm 1958
Echinoderes caribiensis Kirsteuer, 1964	Western Atlantic	Mochima Bay, Venezuela	Kirsteuer 1964
Echinoderes horni Higgins, 1983	Western Atlantic	Carrie Bow Cay, Belize. Kingston Harbor, Jamaica. Icaquitos Bay, Dominican Republic. La Parguera, Puerto Rico.	Higgins 1983 Cepeda et al. 2019a Cepeda et al. 2019c Cepeda 2021
Echinoderes imperforatus Higgins, 1983	Western Atlantic	Carrie Bow Cay, Belize. Guantánamo Bay, Cuba.	Higgins 1983 Cepeda 2021
Echinoderes intermedius Sørensen, 2006	Western Atlantic	Bon Accord, Tobago.	Cepeda 2021
Echinoderes komatsui Yamasaki & Fujimoto, 2014	Western Pacific	Ryukyu Islands, Japan	Yamasaki & Fujimoto 2014 Uozumi et al. 2018

Echinoderes orestauri Pardos et al., 2016	Western Atlantic	Bastimentos Island, Panama	Pardos et al. 2016b
Echinoderes parahorni Cepeda et al., 2019	Western Atlantic	Kingston Harbor, Jamaica. Puerto Príncipe, Haiti. Puerto Blanco and Icaquitos Bay, Dominican Republic.	Cepeda et al. 2019a Cepeda 2021
Echinoderes spinifurca Sørensen et al., 2015	Western Atlantic	Puerto Blanco, Dominican Republic	Cepeda et al. 2019a Cepeda 2021
Echinoderes strii Pardos et al., 2016	Eastern Pacific	Pedro González Island, Panama	Pardos et al. 2016a
Echinoderes sublicarum Higgins, 1977	Western Atlantic	Kingston Harbor, Jamaica. Margarita Island, Venezuela.	Cepeda 2021
Echinoderes teretis Brown, 1999 in Adrianov & Malakhov, 1999	Western Pacific	Broken Bay, Australia	Adrianov & Malakhov 1999
Echinoderes truncatus Higgins, 1983	Western Atlantic	Carrie Bow Cay, Belize	Higgins 1983
Echinoderes wallaceae Higgins, 1983	Western Atlantic	Carrie Bow Cay, Belize. Guantánamo Bay, Cuba.	Higgins 1983 Cepeda 2021
Fujuriphyes deirophorus (Higgins, 1983)	Western Atlantic	Carrie Bow Cay, Belize	Higgins 1983
Fujuriphyes distentus (Higgins, 1983)	Western Atlantic	Carrie Bow Cay, Belize	Higgins 1983
Higginsium erismatum (Higgins, 1983)	Western Atlantic	Carrie Bow Cay, Belize	Higgins 1983
Higginsium trisetosum (Higgins, 1983)	Western Atlantic	Carrie Bow Cay, Belize	Higgins 1983
Leiocanthus corrugatus (Higgins, 1983)	Western Atlantic	Carrie Bow Cay, Belize	Higgins 1983
Leiocanthus ecphantor (Higgins, 1983)	Western Atlantic	Carrie Bow Cay, Belize	Higgins 1983
Leiocanthus emarginatus (Higgins, 1983)	Western Atlantic	Carrie Bow Cay, Belize	Higgins 1983
Paracentrophyes praedictus Higgins, 1983	Western Atlantic	Carrie Bow Cay, Belize	Higgins 1983
Pycnophyes alexandroi Pardos et al., 2016	Western Atlantic	Bocas del Toro, Panama	Pardos et al. 2016b
Pycnophyes apotomus (Higgins, 1983)	Western Atlantic	Carrie Bow Cay, Belize	Higgins 1983
Pycnophyes stenopygus (Higgins, 1983)	Western Atlantic	Carrie Bow Cay, Belize	Higgins 1983
Setaphyes iniorhaptus (Higgins, 1983)	Western Atlantic	Carrie Bow Cay, Belize	Higgins 1983
Sphenoderes indicus Higgins, 1969	Indian	Bay of Bengal	Higgins 1969

Table 2. Morphological measurements and dimensions (in µm) of adult specimens of *Echinoderes cyaneafictus* sp. nov. from the type locality, including number of measured specimens (*n*), mean value and standard deviation (Sd) of each feature, depicted for the holotype and all the type series. Abbreviations: ac, acicular spine; LA, lateral accessory; LD, laterodorsal; LTAS, lateral terminal accessory spine length; LTS, lateral terminal spine length; LV, lateroventral; MD, middorsal; MSW, maximum sternal width; S, segment length; SL, sublateral; SW, standard sternal width; t, tube; TL, total trunk length; numbers after abbreviations indicate the corresponding segment.

Character	Holotype	Range	Mean	Sd, *n*
TL	250.6	194.1–268.7	231.2	21.9, 29
MSW-7	45.1	39.6–46.6	44.5	1.4, 27
MSW-7/TL (%)	18.0	16.6–23.3	19.4	1.8, 27
SW-10	39.9	37.5–41.6	39.6	1.0, 28
SW-10/TL (%)	15.9	14.6–20.8	17.3	1.8, 28
S1	21.6	17.7–28.6	22.1	3.0, 30
S2	21.2	16.5–23.7	20.4	2.1, 30
S3	17.9	13.9–26.8	19.7	2.9, 30
S4	24.7	17.9–27.9	23.0	2.7, 29
S5	29.3	20.0–32.7	25.2	3.0, 30
S6	36.6	21.5–36.6	27.0	3.8, 30
S7	32.8	24.0–40.8	30.6	4.0, 30
S8	33.0	23.8–39.8	33.9	4.1, 30
S9	40.4	27.2–44.6	37.2	3.8, 30
S10	36.5	28.8–37.8	33.7	2.4, 29
S11	25.3	22.0–32.3	27.2	2.7, 29
MD4 (ac)	5.3	4.2–10.2	6.5	1.7, 24
LV5 (t)	9.2	6.9–11.7	9.5	1.3, 23
SL6 (ac)	5.7	4.0–6.6	5.1	0.7, 28
SL7 (ac)	5.1	4.6–7.6	5.7	0.7, 27
LA8 (t)	9.0	7.7–14.8	11.7	2.0, 26
LD10 (t)	12.7	10.3–14.9	12.2	1.5, 8
LTS	56.4	51.4–59.0	54.9	2.0, 29
LTS/TL (%)	22.5	20.3–28.5	23.8	2.3, 29
LTAS	/	9.4–12.7	11.1	1.0, 12
LTAS/LTS (%)	/	4.4–5.8	5.0	0.5, 12

968 **Table 3**. Summary of nature and arrangement of spines, tubes, sensory spots, glandular
969 cell outlets and nephridiopores in adults of *Echinoderes cyaneafictus* sp. nov.
970 Abbreviations: ac, acicular spine; dss, droplet-shaped sensory spot; gcoI, type 1 glandular
971 cell outlet; LD, laterodorsal; ltas, lateral terminal accessory spine; lts, lateral terminal
972 spine; LV, lateroventral; MD, middorsal; ML, midlateral; ne, nephridiopore; PD,
973 paradorsal; ps, penile spines; rss, rounded sensory spot; SD, subdorsal; SL, sublateral; t,
974 tube; VL, ventrolateral; VM, ventromedial; ♂/♀ indicate sexually dimorphic structures.

Segment	MD	PD	SD	LD	ML	SL	LA	LV	VL	VM
1	gcoI		rss	rss				gcoI	rss	
2	gcoI, dss (♂)	dss (♀)	dss	dss	dss (♀)					gcoI, dss
3	gcoI, dss		dss		dss (♀)					gcoI, dss
4	ac	gcoI								gcoI
5		gcoI	dss		dss			t		gcoI, dss
6		gcoI	dss		dss	ac				gcoI, dss
7		gcoI	dss		dss	ac				gcoI, dss
8		gcoI, dss					t		dss	gcoI
9		gcoI, dss	dss			ne			dss	gcoI
10	gcoI, gcoI		dss	t					dss	gcoI
11	gcoI		rss					lts, ps x3 (♂), ltas (♀)		rss

975
976
977
978
979
980
981
982
983
984
985
986
987
988
989
990
991
992
993

Table 4. Morphological measurements and dimensions (in µm) of adult specimens of *Echinoderes parthenope* sp. nov. from the type locality, including number of measured specimens (*n*), mean value and standard deviation (Sd) of each feature, depicted for the holotype and all the type series. Abbreviations: ac, acicular spine; LA, lateral accessory; LD, laterodorsal; LTAS, lateral terminal accessory spine length; LTS, lateral terminal spine length; LV, lateroventral; MD, middorsal; MSW, maximum sternal width; S, segment length; SL, sublateral; SW, standard sternal width; t, tube; TL, total trunk length; numbers after abbreviations indicate the corresponding segment.

Character	Holotype	Range	Mean	Sd, *n*
TL	310.7	217.0–312.9	285.5	30.4, 7
MSW-8	57.0	57.0–66.7	61.5	2.4, 7
MSW-8/TL (%)	18.3	18.3–28.3	21.9	2.2, 7
SW-10	35.5	35.5–55.3	48.5	5.3, 7
SW-10/TL (%)	11.4	11.4–21.4	17.3	2.6, 7
S1	31.7	26.4–37.8	33.1	2.8, 7
S2	25.2	19.9–28.4	23.9	2.7, 7
S3	25.3	19.7–29.9	25.1	2.8, 7
S4	27.9	22.2–38.4	28.7	3.9, 7
S5	29.6	22.5–32.5	28.7	3.0, 7
S6	31.7	21.8–35.1	30.8	4.8, 7
S7	36.3	29.8–40.8	36.7	3.5, 7
S8	44.1	44.1–49.5	46.7	1.9, 7
S9	51.2	51.2–59.8	54.9	2.8, 7
S10	26.2	24.0–36.9	29.1	4.8, 7
S11	24.5	20.2–26.5	23.4	1.4, 7
MD4 (ac)	6.1	6.1–10.6	8.6	1.6, 6
LV5 (t)	21.4	14.7–28.5	20.3	3.6, 7
LV6 (ac)	4.3	4.3–9.0	6.2	1.1, 7
SL7 (ac)	3.4	3.4–8.2	6.1	1.2, 7
SL8 (t)	22.8	19.5–24.6	22.3	1.4, 7
LA8 (ac)	7.3	5.0–9.9	7.6	0.8, 7
LD10 (t)	18.5	16.5–35.9	21.6	5.3, 6
LTS	154.1	134.7–160.5	148.9	7.8, 7
LTS/TL (%)	49.6	43.4–62.4	52.9	5.4, 7
LTAS	/	/	16.3	0.0, 1
LTAS/LTS (%)	/	/	10.1	0.0, 1

Table 5. Summary of nature and arrangement of spines, tubes, sensory spots, glandular cell outlets, nephridiopores and other cuticular structures in adults of *Echinoderes parthenope* sp. nov. Abbreviations: ac, acicular spine; ce, cuticular extension; cp, cuticular process; dss, droplet-shaped sensory spot; gcoI/II, glandular cell outlet type 1/2; LA, lateral accessory; LD, laterodorsal; ltas, lateral terminal accessory spine; lts, lateral terminal spine; LV, lateroventral; MD, middorsal; ML, midlateral; ne, nephridiopore; PD, paradorsal; ps, penile spines; rss, rounded sensory spot; SD, subdorsal; SL, sublateral; th, tuft of hairs; t, tube; VL, ventrolateral; VM, ventromedial; ♂/♀ indicate sexually dimorphic structures.

Segment	MD	PD	SD	LD	ML	SL	LA	LV	VL	VM
1	gcoI		rss	rss				gcoI, rss		
2			dss	dss					dss	
3			dss		dss					
4	ac		dss (♂)		gcoII					
5			gcoII		dss			t		gcoI, dss
6			gcoII, dss		dss		gcoII	ac		gcoI, dss
7			dss		dss	gcoII, ac				gcoI, dss
8			dss			t	ac			gcoI, dss
9		dss	dss	gcoII	dss	ne			dss	gcoI
10	gcoI, gcoI		ce (♂), th (♀)	t (♂)						
11	gcoI, cp (♂)						ltas (♀)	lts, ps x3 (♂)		

1039 **FIGURE CAPTIONS.**

1040 Figure 1. Map showing the location of the study site in the Indian Ocean (A), the Comoros
1041 Archipelago (B), the Mayotte Archipelago (C) and the Chirongui Bay (D). An illustration
1042 of the study site structure is represented in the horizontal profile (E). The mangrove cover
1043 was mapped by photo-interpretation and manual digitizing by D. Cepeda using the
1044 Adobe® Photoshop CS6 software.

1045 Figure 2. Line art drawing of *Echinoderes cyaneafictus* sp. nov. A: Ventral male
1046 overview; B: Dorsal male overview; C: Dorsal female overview of segments 10–11. D:
1047 Ventral female overview of segments 1–3. E: Dorsal female overview of segments 1–3.
1048 Abbreviations: dpl; dorsal placid; epo, enlarged pore; lat, lateral accessory tube; ldrss,
1049 laterodorsal rounded sensory spot; ldt, laterodorsal tube; lts, lateral terminal spine;
1050 lvgco1, lateroventral type 1 glandular cell outlet; mddss, middorsal droplet-shaped
1051 sensory spot; mdgco1, middorsal type 1 glandular cell outlet; mds, middorsal spine;
1052 mldss, midlateral droplet-shaped sensory spot; mvpl, midventral placid; pddss, paradorsal
1053 droplet-shaped sensory spot; pdgco1, paradorsal type 1 glandular cell outlet; ppf, primary
1054 pectinate fringe; ps; penile spine (followed by number of corresponding pair); S, segment
1055 (followed by number of corresponding segment); sddss; subdorsal droplet-shaped sensory
1056 spot; sdrss, subdorsal rounded sensory spot; slne, sublateral nephridiopore; sls, sublateral
1057 spine; te, tergal extension; tp, trichoscalid plate; vldss, ventrolateral droplet-shaped
1058 sensory spot; vmdss, ventromedial droplet-shaped sensory spot; vmgco1, ventromedial
1059 type 1 glandular cell outlet; vmrss, ventromedial rounded sensory spot.

1060 Figure 3. Light micrographs of male holotype MNHN-623Ma (A-B, D), and female
1061 paratype MNHN-602Ma (C, E-F) of *Echinoderes cyaneafictus* sp. nov., showing trunk
1062 overview and details on the head, neck, and segments 1–8. A: Ventral trunk overview; B:
1063 Dorsal view on segments 1–4; C: Midlateral to ventrolateral view on left side of cuticular
1064 plates of segments 5–8; D: Ventral view on segments 1–4; E: Detail of elongated
1065 micropapillae sensory spot on segment 1; F: Mouth cone and introvert. Abbreviations:
1066 ba, bacteria; bs, basal sheath; dpl, dorsal placid; ep, distal end-piece; lat, lateral accessory
1067 tube; ldess, laterodorsal elongated micropapillae sensory spot; lvt, lateroventral tube;
1068 mds, middorsal spine; mvpl, midventral placid; oos, outer oral style; phc, pharyngeal
1069 crown; ppf, primary pectinate fringe; psc, primary spinoscalid; rsc, regular-sized scalid;
1070 sdess, subdorsal elongated micropapillae sensory spot; sls, sublateral spine; tsp,
1071 trichoscalid plate; vmess, ventromedial elongated micropapillae sensory spot; numbers
1072 after abbreviations indicates corresponding segment; glandular cell outlets are marked as
1073 continuous circles, and sensory spots as dashed circles/droplet-shaped figures.

1074 Figure 4. Light micrographs of male holotype MNHN-623Ma (B-C, E), male paratype
1075 MNHN-599Ma (A), and female paratypes MNHN-602Ma (D) and MNHN-616Ma (F) of
1076 *Echinoderes cyaneafictus* sp. nov., showing trunk overview and details on the
1077 nephridiopore and segments 5–11. A: Ventral trunk overview; B: Dorsal view on
1078 segments 5–8; C; Dorsal view on segments 8–10; D: Lateral terminal and lateral
1079 accessory terminal spines; E: Ventral view on segments 10–11; F: Overview of
1080 nephridiopore in midlateral view. Abbreviations: epo, enlarged pore; f, female condition
1081 of sexually dimorphic character; ltas, lateral terminal accessory spines; lts, lateral
1082 terminal spines; m, male condition of sexually dimorphic character; mlne, midlateral

nephridiopore; ppf, primary pectinate fringe; ps, penile spine; te, tergal extension; glandular cell outlets are marked as continuous circles, and sensory spots as dashed circles/droplet-shaped figures.

Figure 5. Line art drawing of *Echinoderes parthenope* sp. nov. A: Ventral male overview; B: Dorsal male overview; C: ventral female overview of segments 10–11; D: dorsal female overview of segments 10–11. Abbreviations: dpl, dorsal placid; lagco2, lateral accessory type 2 glandular cell outlet; las, lateral accessory spine; ldt, laterodorsal tube; ltas, lateral terminal accessory spine; lts, lateral terminal spine; lvgco1, lateroventral type 1 glandular cell outlet; lvs, lateroventral spine; lvt, lateroventral tube; mdgco1, middorsal type 1 glandular cell outlet; mds, middorsal spine; mldss, midlateral droplet-shaped sensory spot; mlgco2, midlateral type 2 glandular cell outlet; mvpl, midventral placid; pc, pachycyclus; pddss, paradorsal droplet-shaped sensory spot; ppf, primary pectinate fringe; ps, penile spine (followed by number of corresponding pair); S, segment (followed by number of corresponding segment); sdce, subdorsal cuticular extension; sddss, subdorsal droplet-shaped sensory spot; sdgco2, subdorsal type 2 glandular cell outlet; sdrss, subdorsal rounded sensory spot; sdth, subdorsal tuft of hairs; se, sternal extension; slgco2, sublateral type 2 glandular cell outlet; slne, sublateral nephridiopore; sls, sublateral spine; slt, sublateral tube; te, tergal extension; tsp, trichoscalid plate; vldss, ventrolateral droplet-shaped sensory spot; vmdss, ventromedial droplet-shaped sensory spot; vmgco1, ventromedial type 1 glandular cell outlet.

Figure 6. Light micrographs of male holotype MNHN-613Ma (E), male paratypes MNHN-649Ma (B-C) and MNHN-651Ma (G), and female paratype MNHN-637Ma (A, D, F, H) of *Echinoderes parthenope* sp. nov. showing trunk overviews and details on the head, neck, nephridiopore and lateral terminal spines. A: Dorsal trunk overview; B: Mouth cone; C: Introvert; D: Ventral neck view: E: lateral terminal spines; F: detail of nephridiopore in midlateral view; G: overview of nephridiopore in midlateral view; H: ingested diatoms. Abbreviations: aa (sp), anterior area of nephridiopore (sieve plate); bfs, basal fringed sheath; bs, basal sheath; ep, distal end-piece; epo, enlarged pore; lts, lateral terminal spines; mlne, midlateral nephridiopore; mvpl, midventral placid; oos, outer oral style; pa, posterior area of nephridiopore; phc, pharyngeal crown; psc, primary spinoscalid; rsc, regular-sized scalid; tsp, trichoscalid plate.

Figure 7. Light micrographs of male holotype MNHN-613Ma (A, D, F-G), male paratype MNHN-641Ma (C) and female paratype MNHN-637Ma (B, E) of *Echinoderes parthenope* sp. nov. showing cuticular details of segments 1–8. A: Dorsal and lateral overview of neck and segments 1–4; B: Dorsal view of neck and segments 1–4; C: midlateral to ventromedial view on right side of cuticular plates of segments 1–4; D: middorsal to midlateral view on right side of tergal plates of segments 5–6; E: midlateral to lateroventral view on left side of tergal plates of segments 5–8; F: midlateral to ventromedial view on right side of cuticular plates of segments 5–6; G: ventral view of segment 8. Abbreviations: dpl, dorsal placid; gco2, type 2 glandular cell outlet; las, lateral accessory spine; lvs, lateroventral spine; lvt, lateroventral tube; m, male condition of sexually dimorphic character; mds, middorsal spine; mls, midlateral spine; mvpl, midventral placid; ppf, primary pectinate fringe; slt, sublateral tube; glandular cell outlets are marked as continuous circles, and sensory spots as dashed circles/droplet-shaped figures.

Figure 8. Light micrographs of male holotype MNHN-613Ma (A-D), male paratype MNHN-642Ma (E) and female paratype MNHN-637Ma (F-G) of *Echinoderes parthenope* sp. nov. showing cuticular details of segments 8–11. A: Dorsal view of segments 8–9; B: Ventral view of segments 9–10; C: penile spines; D: dorsal view of segment 11; E: dorsal view of segments 10–11; F: ventral view of segments 10–11; G: ventral view of segments 10–11. Abbreviations: ce, cuticular extension; f; female condition of sexually dimorphic character; gco2, type 2 glandular cell outlet; go, gonopore; ldt, laterodorsal tube; ltas, lateral terminal accessory spine; lts, lateral terminal spine; m, male condition of sexually dimorphic character; ppf, primary pectinate fringe; pr, protuberance; ps, penile spine (followed by number of corresponding pair); se, sternal extension; te, tergal extension; glandular cell outlets are marked as continuous circles, and sensory spots as dashed circles/droplet-shaped figures.

Figure 9. Scanning electron micrographs of male additional specimen of *Echinoderes parthenope* sp. nov. showing trunk overview and cuticular details of trunk segments. A: Lateral trunk overview; B: lateral view of segments 1–3; C: detail of laterodorsal, rounded sensory spot of segment 1; D: detail of middorsal spine of segment 4; E: lateral view of segments 4–6; F: ventral view of segments 5–7; G: detail of subdorsal droplet-shaped sensory spot and type 2 glandular cell outlet of segment 6; H: lateral view of segment 7; I: detail of sublateral tube and lateral accessory spine of segment 8; J: lateral view of segment 9 (inset shows the midlateral sieve plate); K: detail of midlateral, droplet-shaped sensory spot of segment 9; L: lateral view of segment 11. Abbreviations: gco2, type 2 glandular cell outlet; in, introvert; las, lateral accessory spine; ldt, laterodorsal tube; lts, lateral terminal spine; lvt, lateroventral tube; mds, middorsal spine; mls, midlateral spine; ms, muscular scar; ne, neck; pr, protuberance; ps, penile spines; S, segment (followed by numbers of corresponding segments); slt, sublateral tube; te, tergal extensions; glandular cell outlets are marked as continuous circles, and sensory spots as dashed circles/droplet-shaped figures.

Figure 10. Kinorhynch richness (A) as number of species, density (B) as number of individuals per $10cm^2$ and community composition at the two studied sites ("impacted" vs. "control") (C). Boxplots represent the mean value (thick horizontal line within the box), the distributions of 50% of the data (the box), and the highest and lowest values within 95% of the distribution (the whisker). Contribution of each kinorhynch species to the total community is expressed in percentage in relation to the total abundance.

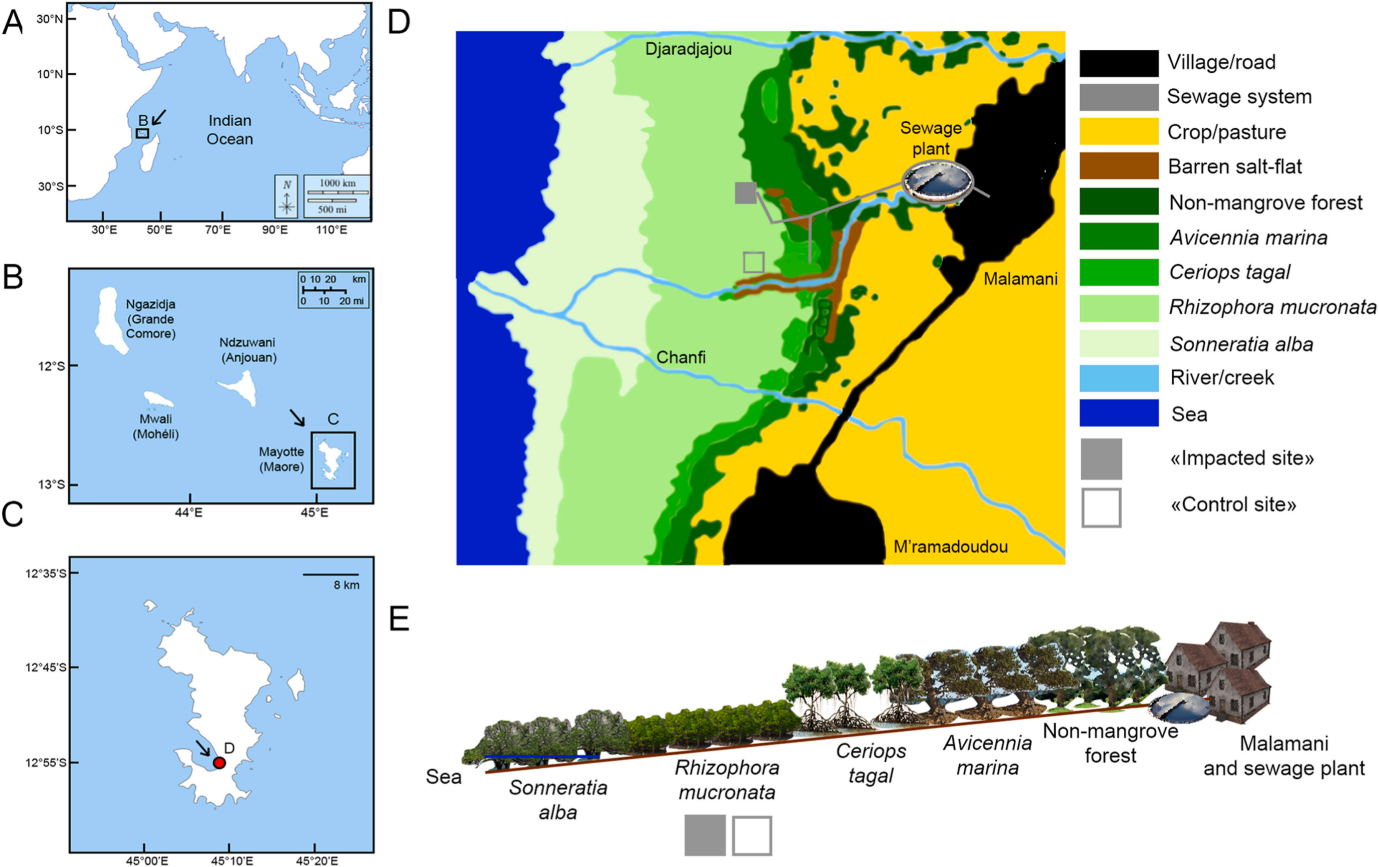
A
30°N
10°N
10°S
30°S
B
Indian
Ocean
N
1000 km
500 mi
30°E
50°E
70°E
90°E
110°E
B
0 10 20 km
0 10 20 mi
Ngazidja
(Grande
Comore)
Ndzuwani
(Anjouan)
Mwali
(Mohéli)
C
Mayotte
(Maore)
12°S
13°S
44°E
45°E
C
12°35'S
12°45'S
12°55'S
8 km
D
45°00'E
45°10'E
45°20'E
D
Djaradjajou
Sewage
plant
Malamani
Chanfi
M'ramadoudou
Village/road
Sewage system
Crop/pasture
Barren salt-flat
Non-mangrove forest
Avicennia marina
Ceriops tagal
Rhizophora mucronata
Sonneratia alba
River/creek
Sea
«Impacted site»
«Control site»
E
Sea
Sonneratia
alba
Rhizophora
mucronata
Ceriops
tagal
Avicennia
marina
Non-mangrove
forest
Malamani
and sewage plant

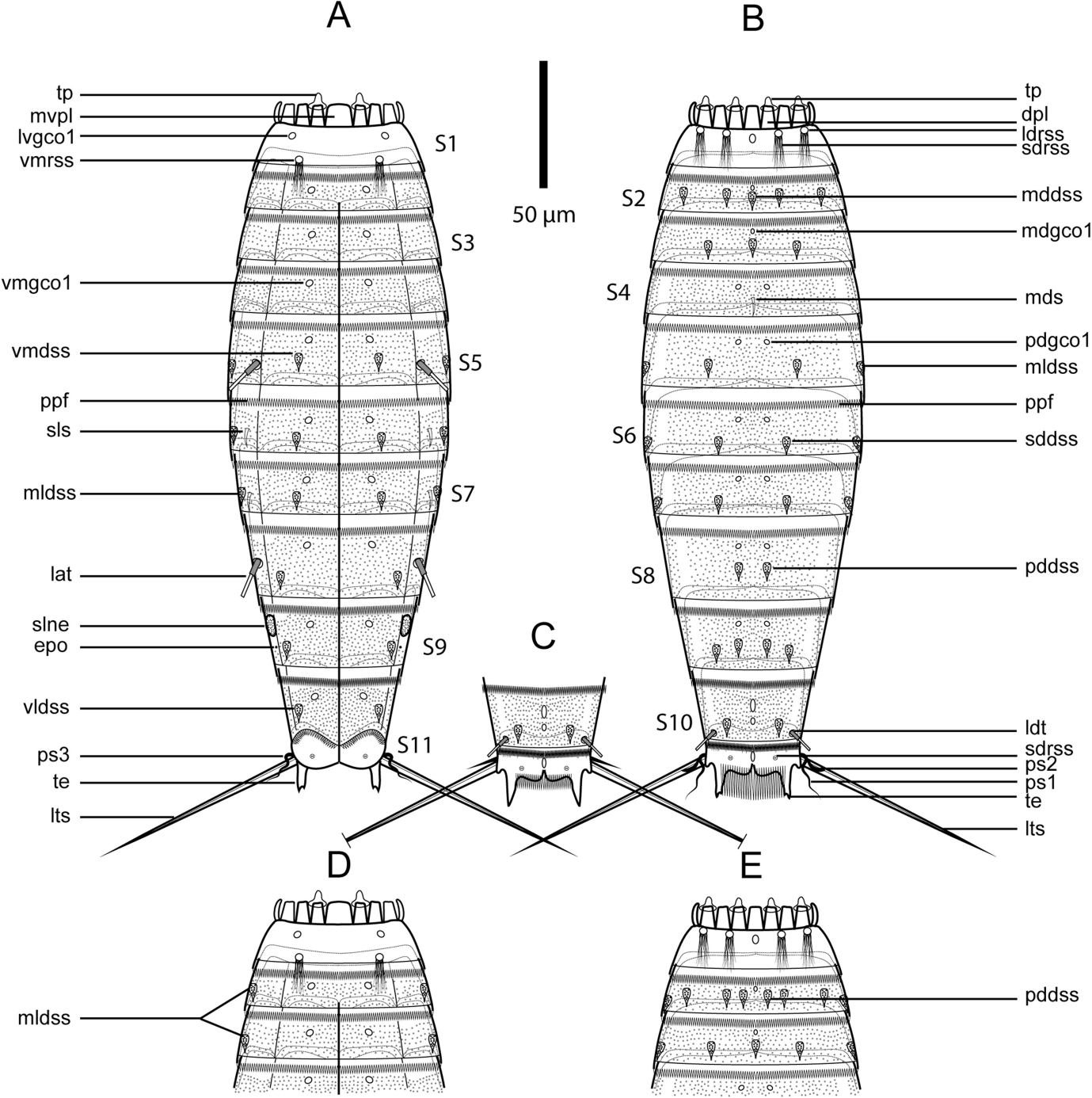
A
B
C
D
E
50 µm
tp
mvpl
lvgco1
vmrss
S1
S3
vmgco1
vmdss
S5
ppf
sls
mldss
S7
lat
slne
epo
S9
vldss
ps3
S11
te
lts
tp
dpl
ldrss
sdrss
S2
mddss
mdgco1
S4
mds
pdgco1
mldss
ppf
S6
sddss
pddss
S8
S10
ldt
sdrss
ps2
ps1
te
lts
mldss
pddss

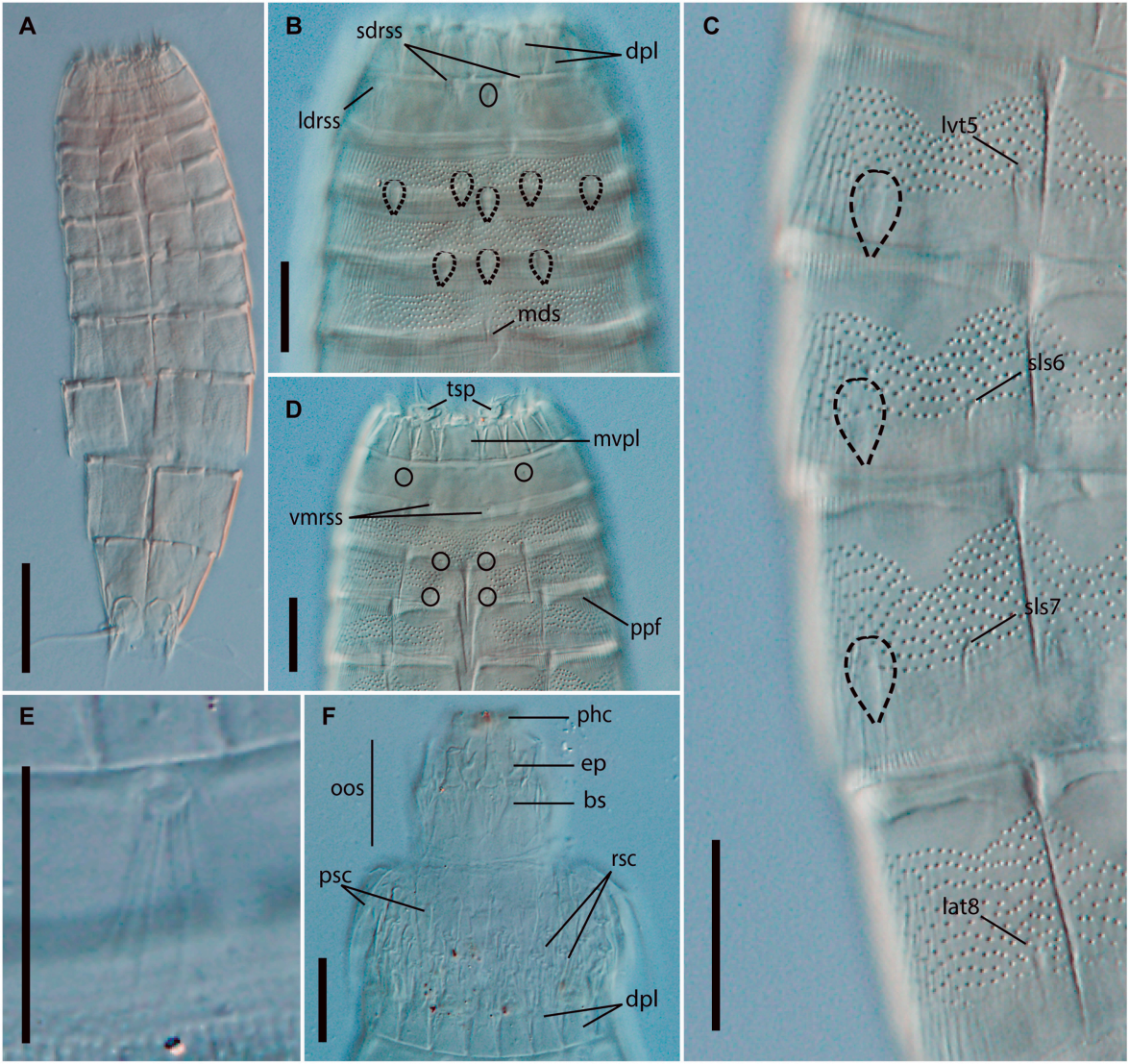
A
B
sdrss
dpl
ldrss
mds
C
lvt5
sls6
sls7
lat8
D
tsp
mvpl
vmrss
ppf
E
F
phc
ep
oos
bs
rsc
psc
dpl

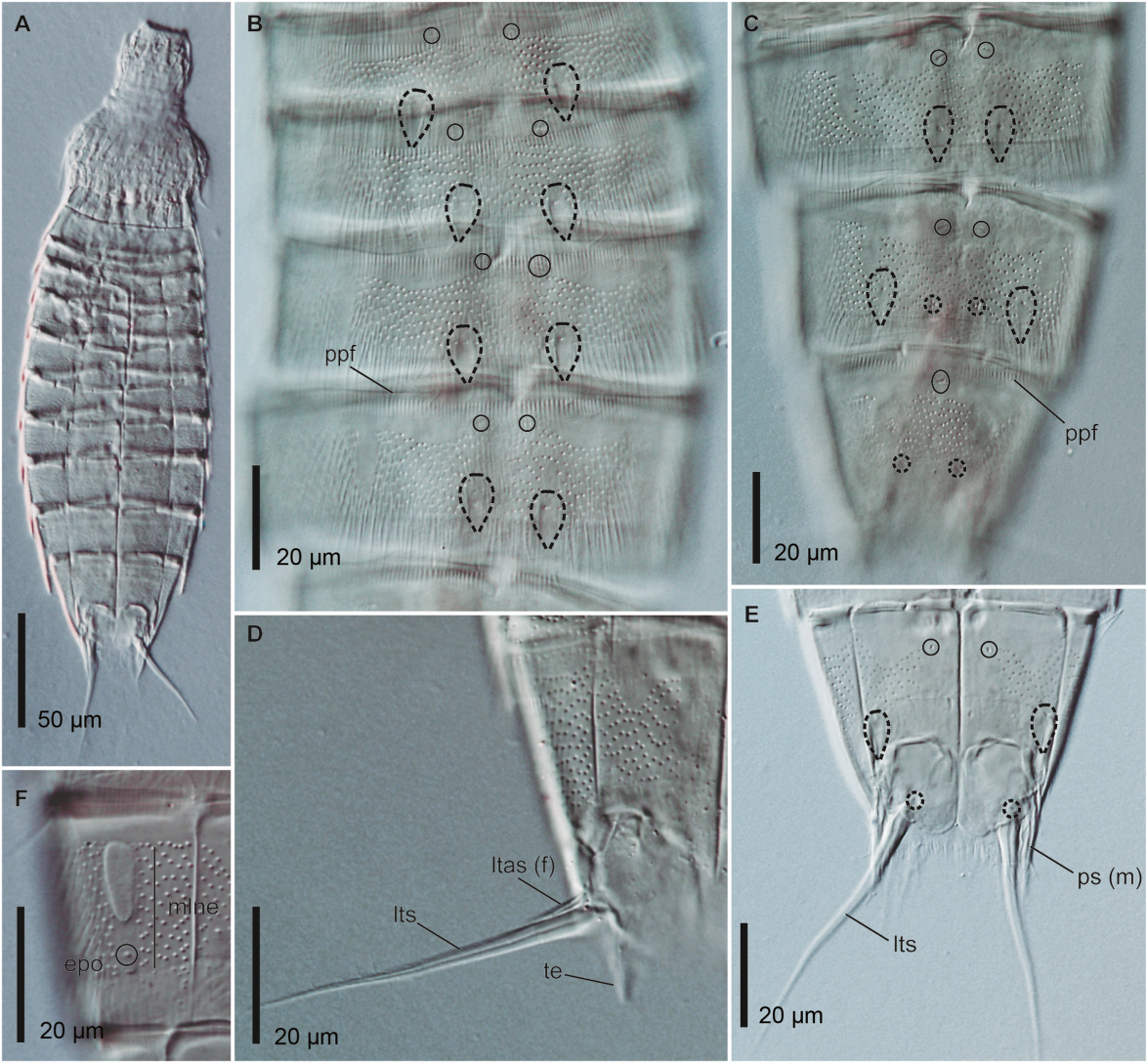
A
50 µm
B
ppf
20 µm
C
ppf
20 µm
D
ltas (f)
lts
te
20 µm
E
ps (m)
lts
20 µm
F
mine
epo
20 µm

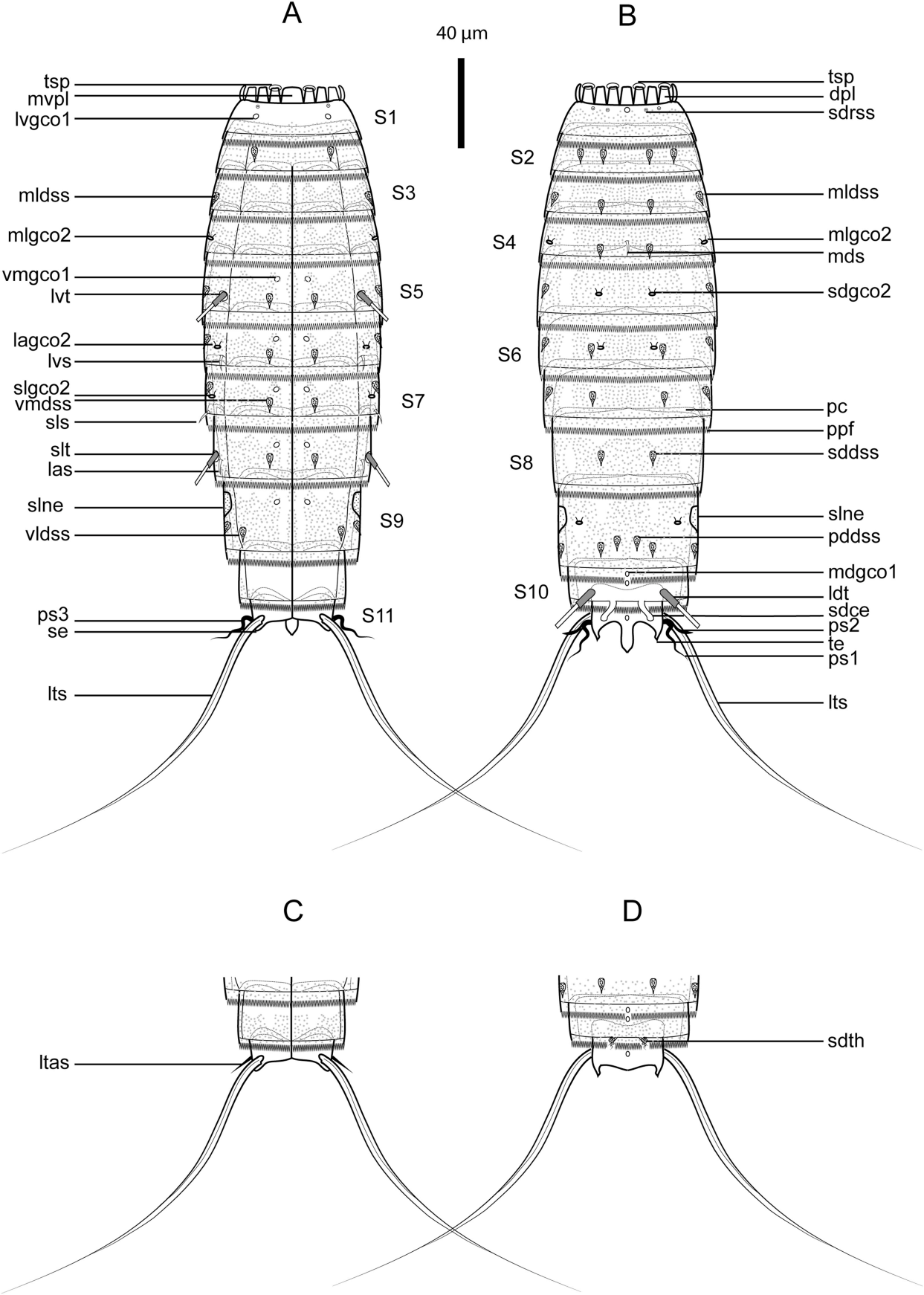
A
B
40 µm
tsp
mvpl
lvgco1
S1
mldss
S3
mlgco2
vmgco1
lvt
S5
lagco2
lvs
slgco2
vmdss
sls
S7
slt
las
slne
vldss
S9
ps3
se
S11
lts
tsp
dpl
sdrss
S2
mldss
S4
mlgco2
mds
sdgco2
S6
pc
ppf
sddss
S8
slne
pddss
mdgco1
S10
ldt
sdce
ps2
te
ps1
lts
C
D
ltas
sdth

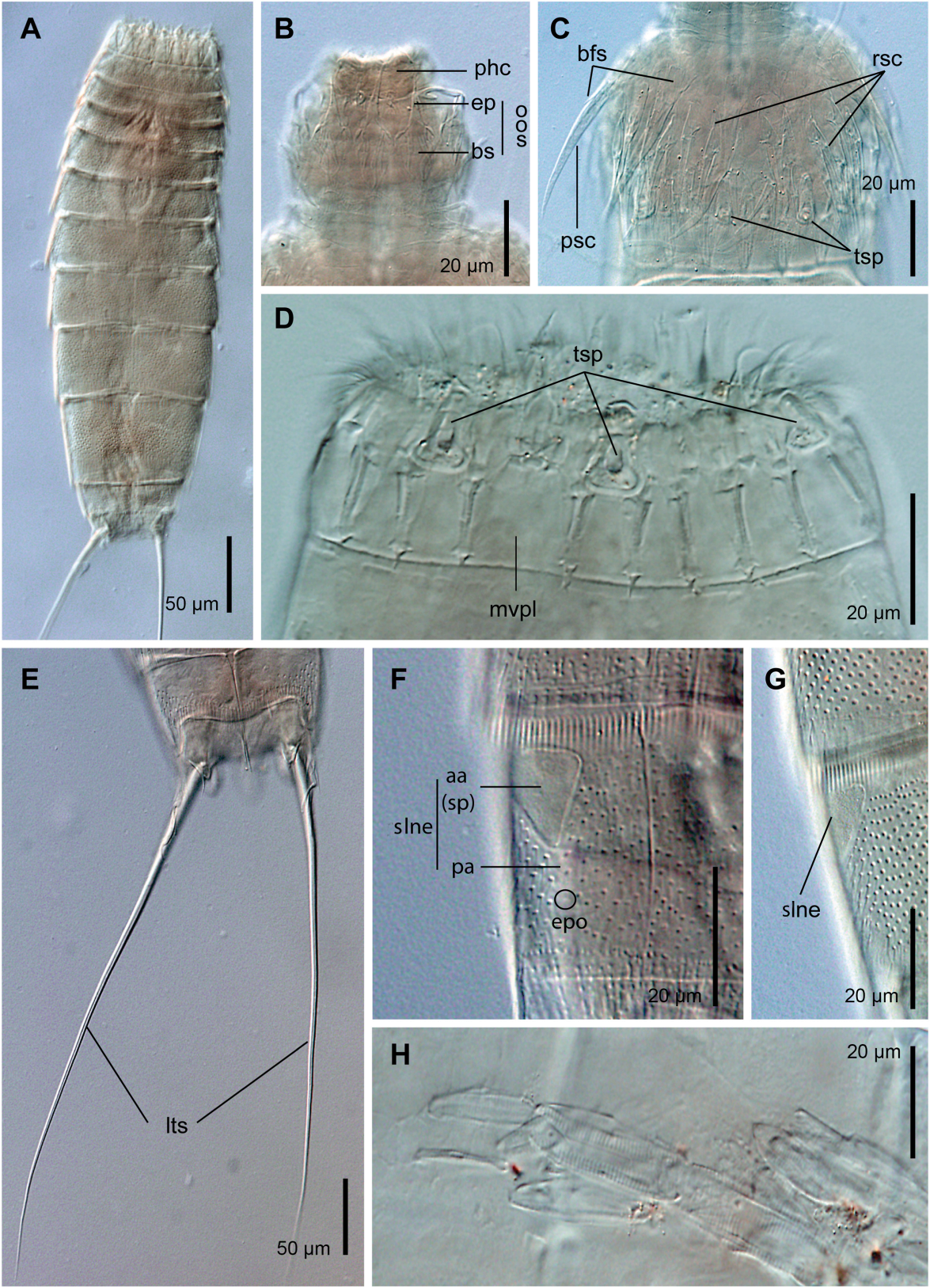
A
50 µm
B
phc
ep
bs
oos
20 µm
C
bfs
rsc
20 µm
psc
tsp
D
tsp
mvpl
20 µm
E
lts
50 µm
F
aa
(sp)
slne
pa
epo
20 µm
G
slne
20 µm
H
20 µm

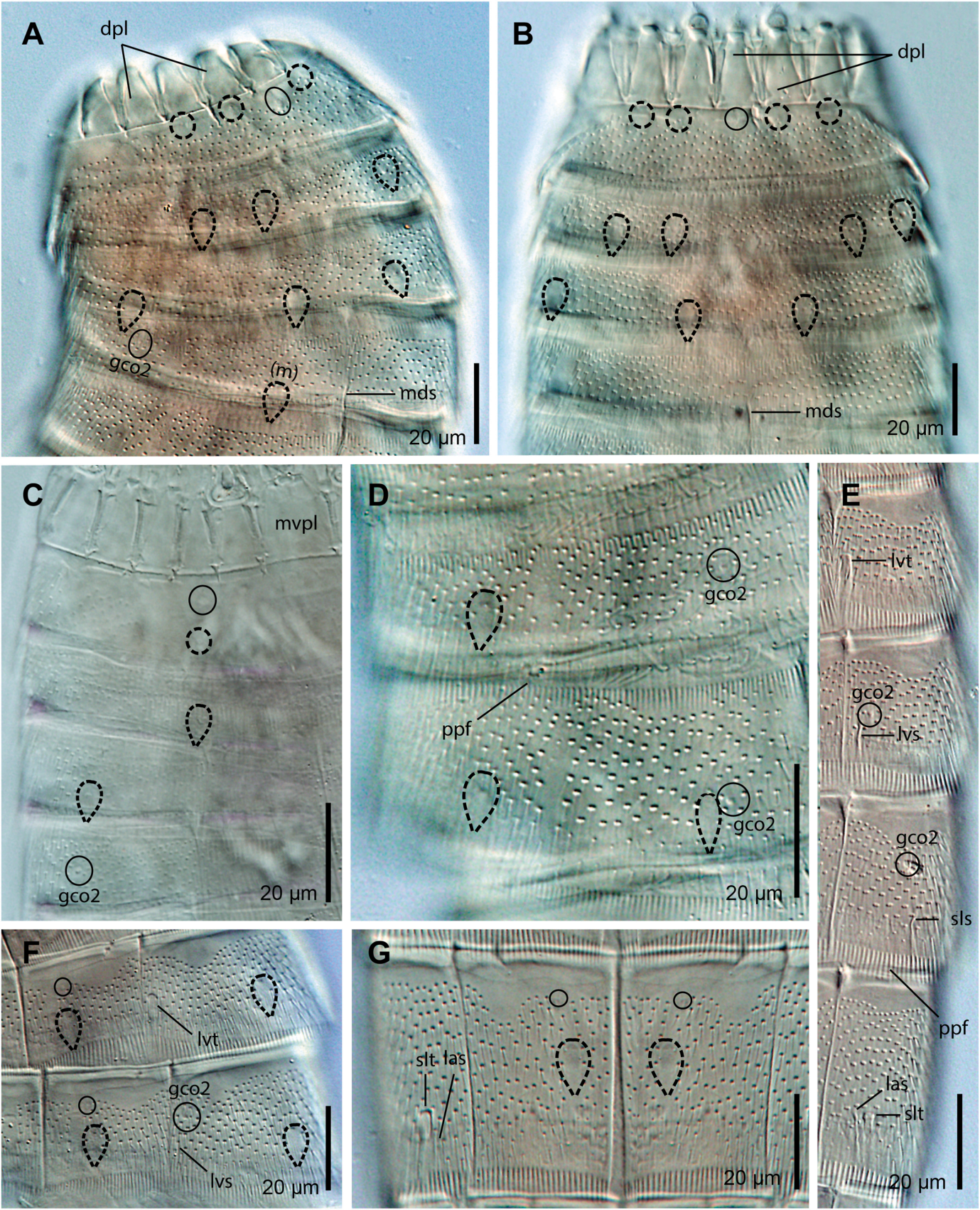
A
dpl
gco2
(m)
mds
20 µm
B
dpl
mds
20 µm
C
mvpl
gco2
20 µm
D
gco2
ppf
gco2
20 µm
E
lvt
gco2
lvs
gco2
sls
ppf
las
slt
20 µm
F
lvt
gco2
lvs
20 µm
G
slt
las
20 µm

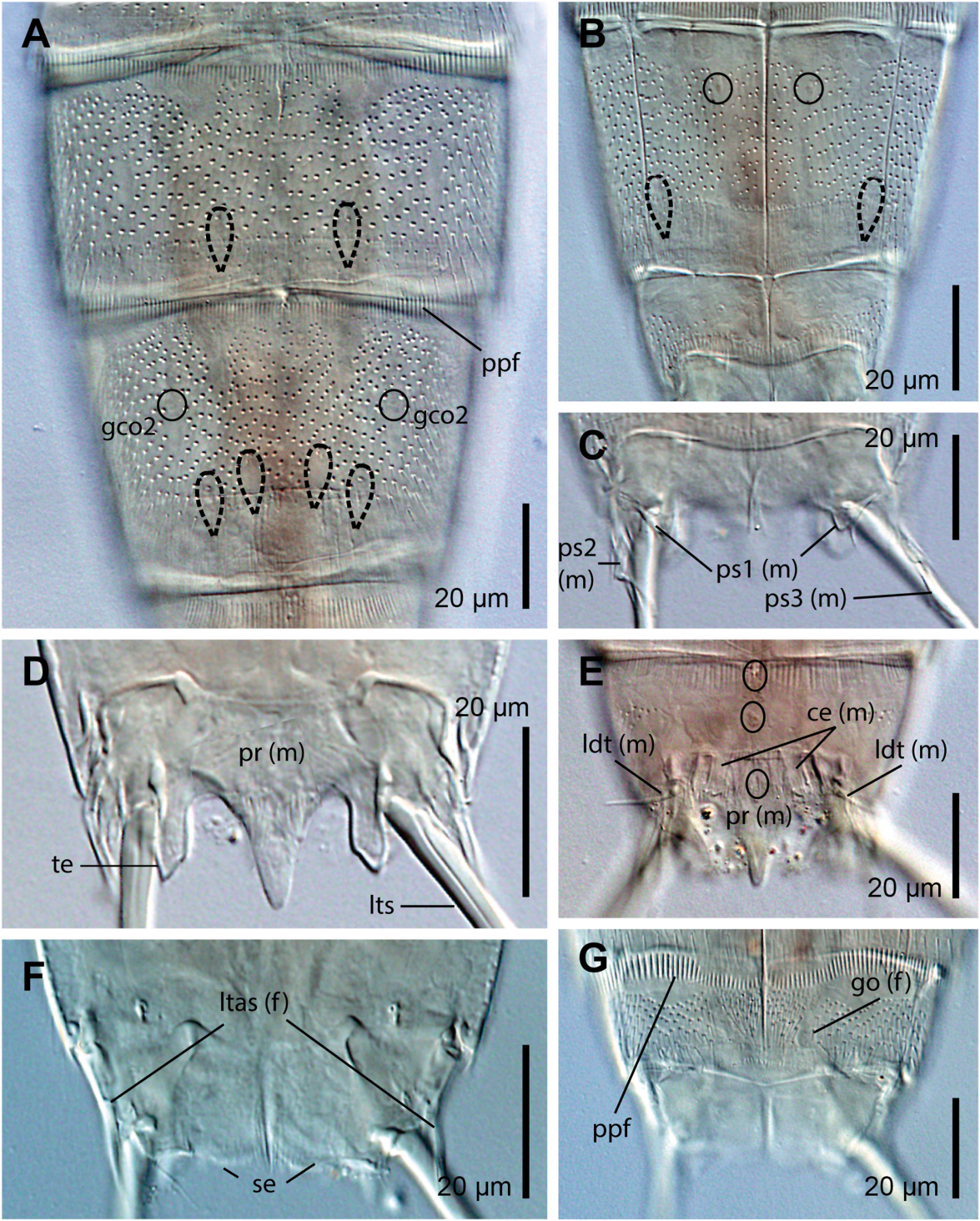
A
ppf
gco2
gco2
20 µm
B
20 µm
C
20 µm
ps2
(m)
ps1 (m)
ps3 (m)
D
20 µm
pr (m)
te
lts
E
ce (m)
ldt (m)
ldt (m)
pr (m)
20 µm
F
ltas (f)
se
20 µm
G
go (f)
ppf
20 µm

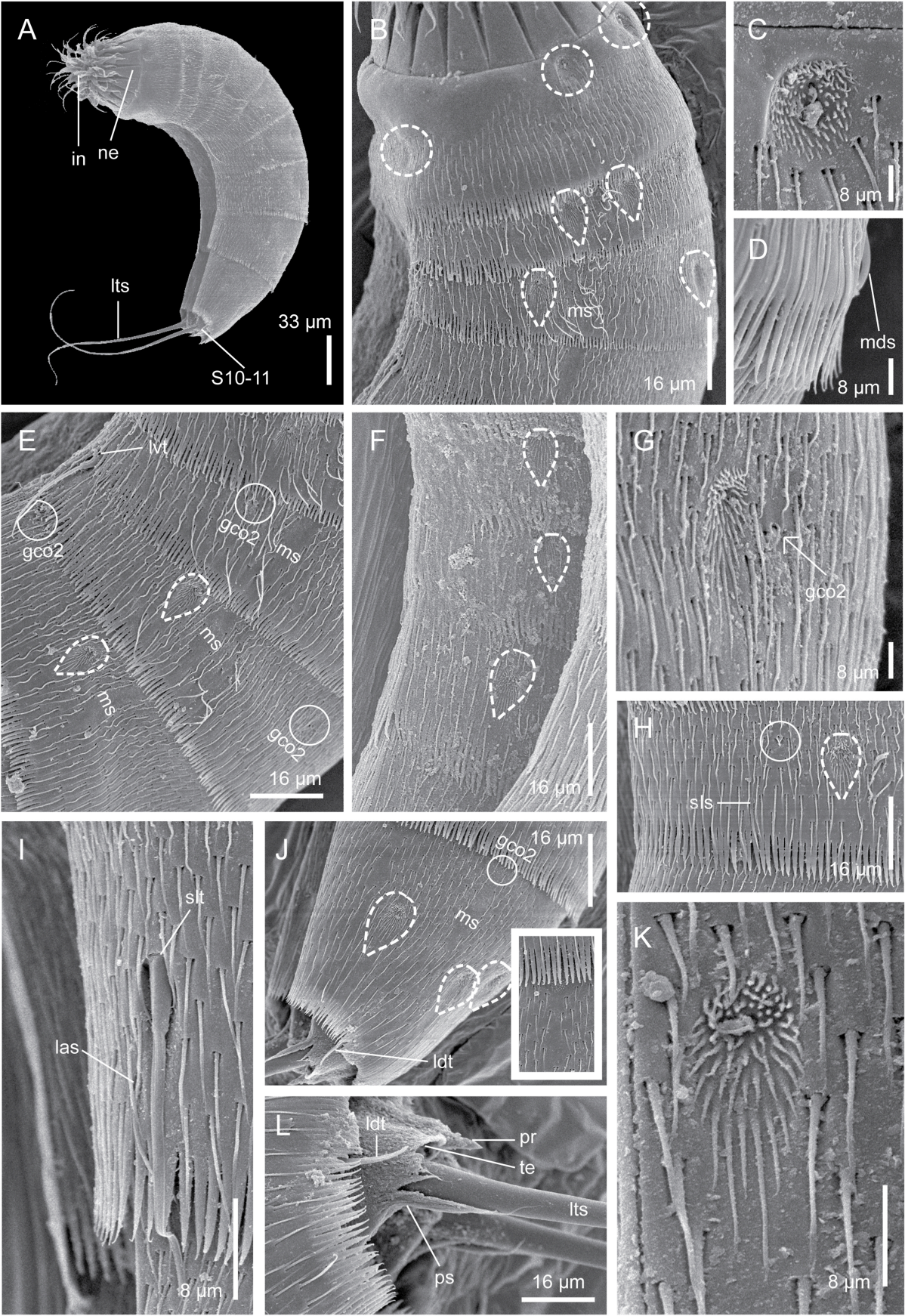
A
in
ne
lts
S10-11
33 µm
B
ms
16 µm
C
8 µm
D
mds
8 µm
E
lvt
gco2
gco2
ms
ms
ms
gco2
16 µm
F
16 µm
G
gco2
8 µm
H
sls
16 µm
I
slt
las
8 µm
J
16 µm
gco2
ms
ldt
K
8 µm
L
ldt
pr
te
lts
ps
16 µm

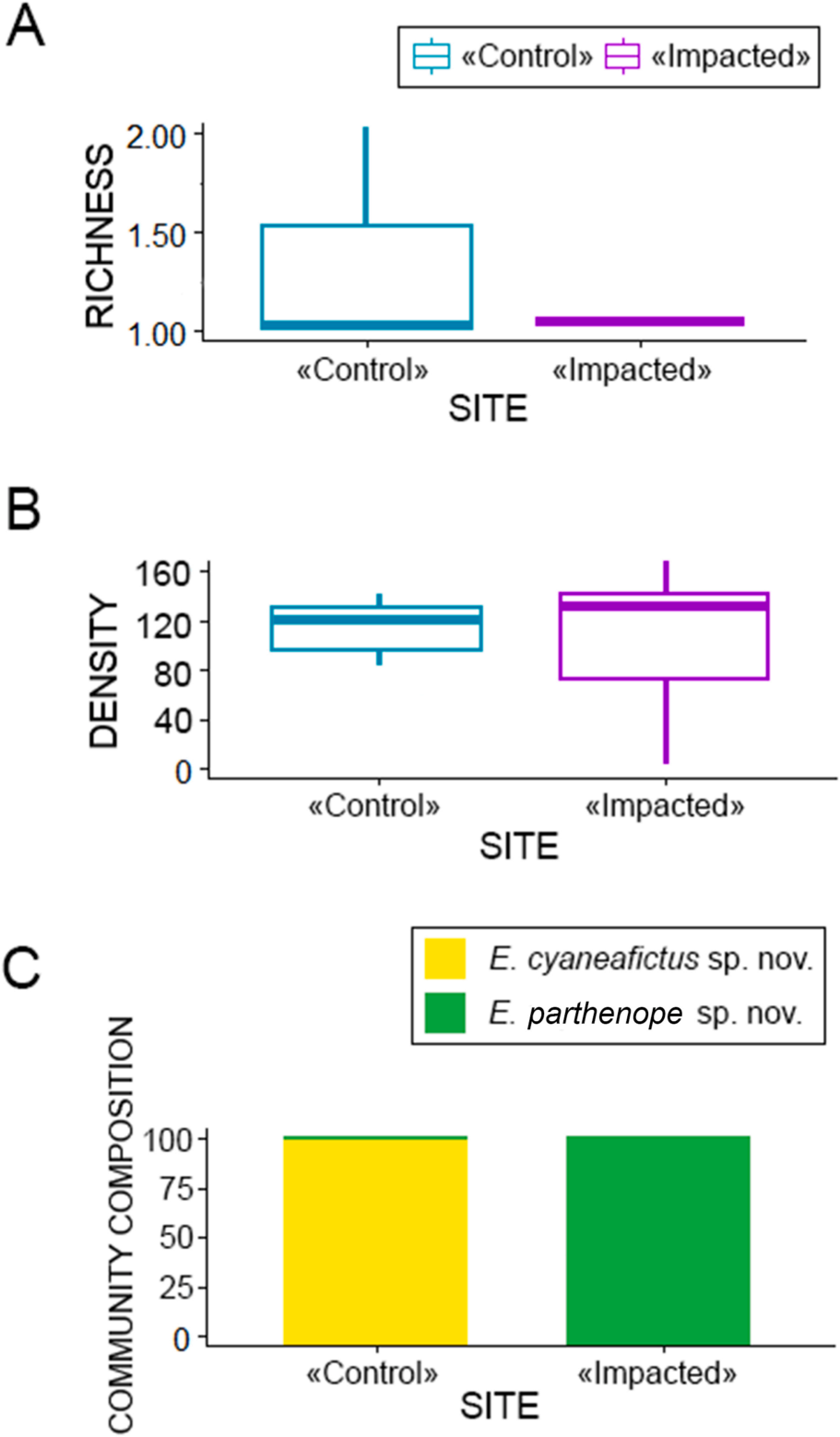
A
«Control»
«Impacted»
RICHNESS
2.00
1.50
1.00
«Control»
«Impacted»
SITE
B
DENSITY
160
120
80
40
0
«Control»
«Impacted»
SITE
C
E. cyaneafictus sp. nov.
E. parthenope sp. nov.
COMMUNITY COMPOSITION
100
75
50
25
0
«Control»
«Impacted»
SITE

Declaration of interests

☒The authors declare that they have no known competing financial interests or personal relationships that could have appeared to influence the work reported in this paper.

☐The authors declare the following financial interests/personal relationships which may be considered as potential competing interests: